Appendix R—Compilation of Slip-in-the-Last-Event Data and Analysis of Last Event, Repeated Slip, and Average Displacement for Recent and Prehistoric Ruptures

By Chris Madden,[1] David E. Haddad,[2] J. Barrett Salisbury,[2] Olaf Zielke,[3] J. Ramón Arrowsmith,[2] Ray J.Weldon, II,[4] and Javier Colunga[2]

Introduction

Slip in the last earthquake along a fault, in conjunction with the application of appropriate recurrence models, can be used to estimate the timing and size of future ground-rupturing earthquakes (Scholz, 2002). A simple approach assumes that the next earthquake along a portion of a fault will occur when the last slip has recovered ("time predictable" behavior). Although catalogues of slip measurements for features displaced during surface-rupturing earthquakes have been available for the past half-century, few reliable measurements are available for displacements along older historical, or prehistoric ruptures. Offset at a point along a fault can be measured from preserved offset features, estimated empirically from fault length-width-area scaling relationships, or computed deterministically. Furthermore, the continuity of surface ruptures along fault segments depends on the magnitude of slip and the structural complexity of the fault zone, (for example, Wells and Coppersmith, 1994; Biasi and Weldon, 2006, Wesnousky, 2008). Measurements of slip in the last earthquake or last few events are difficult to use directly in seismic hazard studies for several reasons, including (1) their sparseness, (2) the inherent ambiguity in their representation of discrete slip per event and average slip at depth and along the causative fault, and (3) the uncertainty in associated rupture length (see discussions in McCalpin, 2009; Field and Page, 2011; Salisbury and others, 2012; and Zielke and others, 2012, for example).

Surface slip measurements can be made along some active faults because offsets generated by the last event are usually well preserved by geomorphic features in the landscape. Many new measurements are made possible because of the availability of high-resolution digital topography (LiDAR) and imagery along active faults (for example, Hudnut and others, 2002; Frankel and others, 2007; Oskin and others, 2007; Zielke and others, 2010; Klinger and others, 2011; Salisbury and others, 2012; Zielke and others, 2012, Haddad and others, 2012). In addition, sustained paleoseismic research along active faults in California and elsewhere has

[1] Oregon State University.
[2] Arizona State University.
[3] King Abdullah University of Science and Technology, Saudi Arabia.
[4] University of Oregon.

yielded many point observations of offset in prior earthquakes, yet no comprehensive compilation has been made.

Although the measurement of absolute slip is relatively straightforward, determining the number of earthquakes that occurred to accumulate that offset is not (unless slip measurements are made immediately after the earthquake). A commonly held assumption is that suites of landforms (for example, offset stream channels and debris flow deposits) develop between earthquakes that are repeatedly offset en masse. This process of repeated slip and the development of offset geomorphic features create groups of offsets with similar magnitude along strike (see, for example, Wallace, 1968; Sieh, 1978; Lienkaemper, 2001; Zielke and others, 2010; Klinger and others, 2011). However, direct dating of such landforms and their association with a paleoearthquake record requires specific geological and climatic conditions, thus leading to a paucity of geomorphic records of slip.

In the large-scale earthquake hazard model Uniform California Earthquake Rupture Forecast, version 3 (UCERF3; *http://www.wgcep.org/*), earthquake rupture rates are computed along the discretized California fault network with ~7-km-long subsections (index *s*). Fault subsections are broken into a series of earthquake ruptures (index *r*) for which slip in the *r*th rupture along the *s*th section is termed *Dsr* (Field and Page, 2011). *Dsr* is specified a priori empirically. Slip rate and event rate data are the principal constraints to be satisfied.

In this report, we summarize our compilation of point measurements of slip in prior individual or sequences of earthquakes along high slip rate strike-slip and dip-slip faults in California for input into the time-dependent UCERF3 model (fig. R1, tables R1 and R2 [shown at end of appendix], and supplementary file R1-1; Arrowsmith and others, 2011; Haddad and others, 2011; Madden and others, 2011).

Figure R1. Google Earth overview map of offsets compiled in this appendix. Location markers show individual slip measurement sites. White lines are UCERF3 faults.

The offset data were standardized in a way to archive important values reported for most offsets, which include the measurement uncertainty, a quality rating, and the number of earthquakes contributing to each offset. We used the inferred most recent earthquake offsets to assign slip in the last earthquake to each fault subsection in UCERF3 for which there was as at least one offset value nearby. These assignments are thus independent measures of *Dsr* and can be used in UCERF3 both as direct a priori specifications or as a posteriori consistency checks.

Methods

Background

Past paleoseismic studies used geomorphic offsets to characterize slip in the last event for large fault ruptures. The essential components of these analyses included (1) the measurement of the offset and its uncertainty in the field, from imagery or high-resolution digital topography, (2) a quality assessment for the reconstruction of each offset, and (3) the assumptions used when determining the number of earthquakes recorded by the displaced landform. Starting with Wallace (1968), local minima of offsets along strike are attributed to the most recent earthquake (MRE). Wallace (1968) identified offset channels along the south-central San Andreas Fault (SAF) and developed a conceptual model for their formation, as well as speculated on their fidelity in recording offset. Sieh (1978) measured offset gullies to reconstruct the slip distribution and average displacement created by the 1857 Fort Tejon earthquake. He tabulated the offset measurements and used a scheme to rate his confidence in each measurement based on the geomorphic quality of the offset feature. Lienkaemper (2001) and Zielke and others (2010, 2012) measured offsets using aerial photographs, field observations, and LiDAR data to build upon and modify Sieh's (1978) initial findings for the 1857 event. Zielke and Arrowsmith (2012) present a software toolkit for measuring and rating lateral offsets from LiDAR digital elevation models (DEMs), which standardizes the methodology and allows for inter-user validation.

McGill and Sieh (1991) measured offset landforms along the central and eastern Garlock Fault and characterized clusters of offsets as slip from the last several events, with the smallest cluster representing slip from the last event. Clusters were analyzed by assigning probability density functions (PDFs) to encompass the measurement and associated error for single features and then summing the individual into Cumulative Offset Probability Density functions (COPD; for example, McGill and Sieh, 1991, figure 6). Klinger and others (2011) analyzed dense offset channels along the Fuyun Fault in northwestern China from high-resolution satellite imagery. They rated quality by the number of channels that could be reconstructed along a few fault reaches tens to hundreds of meters long, and they formalized the analysis of the decaying COPD peaks with offset as a "geomorphic preservation factor" (although it has been notable since Wallace's 1968 plotting of offset histograms). Salisbury and others (2012) measured geomorphic offsets in the field and on LiDAR-derived DEMs along the Clark strand of the San Jacinto Fault to characterize slip in the last and prior events. Salisbury and others (2012) attributed lowest minimum slip values to slip in the last event and clusters of larger offset values to slip in prior events. Salisbury and others (2012) also showed that offsets less than about 0.5 m were not recognizable in general for paleoseismic or historical events. Zielke and others (2010), Grant-Ludwig and others (2010), and Akciz and others (2010) point to a discrepancy between the inferred timing of earthquakes and their associated geomorphically determined offsets with the millennial slip rate along the SAF in the Carrizo Plain. This suggests that not all earthquake offsets are uniquely recorded in a sequence of landform offsets, in particular if they vary in

magnitude from event to event. Our analyses of geomorphic offsets for this report are built upon the methods developed in these studies to characterize slip in the last event and repeated slip for large surface rupturing earthquakes.

Assumptions

Our database (see below for our compilation approach) comprises several thousand offset measurements along active faults in California. Most of the offsets come from measurements of landforms displaced by historical ruptures (that is, without the ambiguity of numbers of formative earthquakes), and the majority of the remaining measurements are of displaced landforms examined using LiDAR data. To assign MRE offsets and repeated slip from sequences of displaced landforms, we make three assumptions:

1. The smallest local offset represents slip in the last surface-rupturing event (after Wallace, 1968; Sieh, 1978; McGill and Sieh, 1991; Zielke and others, 2010, 2012; Klinger and others, 2011; and other works). Based on this assumption, we assigned single event offsets (S in supplementary file R1-1) and multiple event offsets (M). Measurements made at or near paleoseismic sites that record the timing of the last event support this assumption (Weldon and others, 2002). Local minimum slip will be a minimum slip value in areas with complex multi-strand fault zones.
2. The production rate of geomorphic features across faults that can be used to measure slip is greater than the earthquake recurrence rate. Therefore, a suite of landforms is offset en masse in each earthquake, generating groups of offsets along each fault reach. If earthquakes occur more frequently than formation of geomorphic features, the lowest minimum slip may reflect more than one event. Likewise, COPD peaks may include more than one earthquake (see discussion in Zielke and others, 2010, 2012).
3. Clusters of geomorphic offset values represent slip from the same event. Clusters of offsets with different mean values represent cumulative offsets from different numbers of events. Clusters of offset features may also reflect variability in slip from a single rupture.

Data Compilation

Our search for offset measurements focused on faults with high slip rates and long time intervals since the last event relative to the average recurrence interval. Slip rate, timing of the last event, and recurrence interval were obtained from past reports by the Working Group on California Earthquake Probabilities, unless more recently published data were available.

Data from the Literature

We searched the literature to determine the availability of offset data for the highest priority faults. We contacted authors of published slip studies to solicit additional data that may exist in unpublished archives, gray literature, or publications in preparation. Existing data compiled for this effort are described in supplementary file R1-1.

Figure R2 summarizes the workflow of our procedure for compiling, visualizing, and analyzing offset measurements. All offset data were compiled into a comprehensive data table following compilation of unpublished offsets from principal investigators (PIs), published offsets from the literature, and performing our own offset measurements. Minor adjustments were made to the table to standardize the format of each column. The formatted table was then ingested by a

Keyhole Markup Language (KML) file generator. Figure R1 presents an overview of the KML files of offsets for each fault as viewed in Google Earth. All KML files are included in supplementary file R1-3.

New Data Gathered for this Compilation

For faults with LiDAR coverage, but limited, poor, or unavailable offset data, we identified reaches with a high potential to preserve geomorphic offsets and made new slip measurements. We made new geomorphic offset measurements for the Elsinore Fault (57 measurements), Garlock Fault (353 measurements), Owens Valley Fault (145 measurements), and the northern creeping section of the San Andreas Fault (47 measurements) using LiDAR-generated DEMs (LiDAR from the San Andreas B4 Project, Earthscope, and the National Center for Airborne Laser Mapping) and a lateral displacement calculator (Zielke and Arrowsmith, 2012; table R1; supplementary file R1-1).

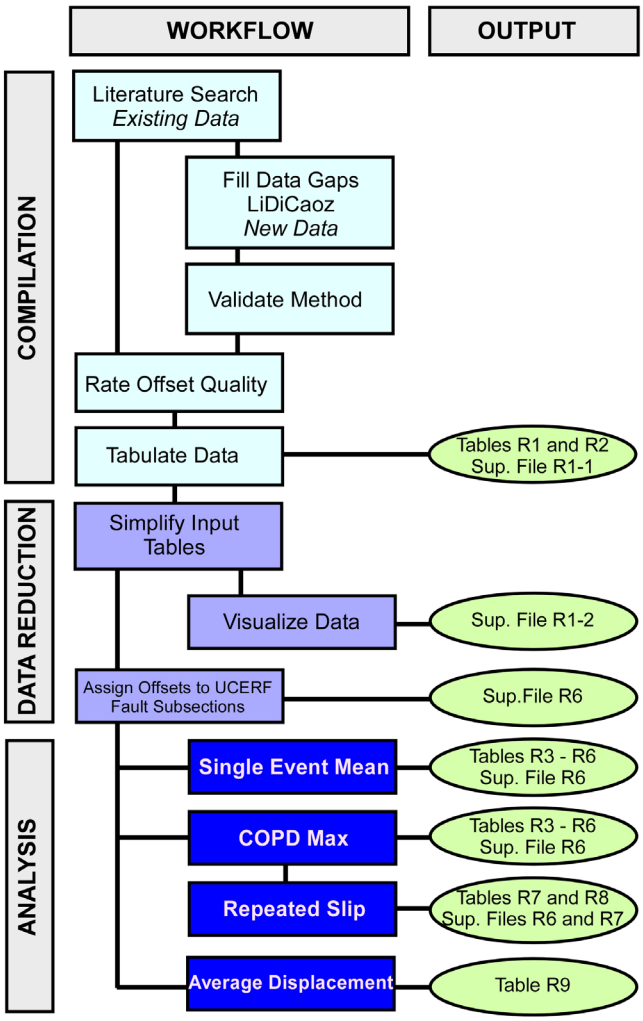

Figure R2. Diagram of workflow to compile, tabulate, reduce, and analyze offset data, and resulting output documented in this report.

LiDAR data were processed at and downloaded from the Open Topography facility (*http://opentopography.org/*), from which submeter-resolution DEMs were created. Using a combination of aerial photographs and topographic slope, relief, and hillshade maps, we digitized fault traces and marked offset features. Each feature was reviewed at least twice to ensure that it is indeed an offset feature and not an artifact of the DEM. Based on the resolution of the available LiDAR data, we felt confident that we could identify features offset 2 m (90-percent chance). Conversely, we feel there is only a small chance (10 percent) of identifying features with 0.25 m offset.

Offset features were analyzed using the lateral displacement calculator to determine optimal, minimum, and maximum slips. Optimal slip values were evaluated by using the goodness-of-fit approach and visually inspected by backslipping the topography using the calculated optimal slip (Zielke and others, 2012). Supplementary file R2-1 details the methodology used to measure offsets using LiDAR DEMs and summarizes offsets that we identified on the Elsinore, Garlock, and Owens Valley Faults. Inter-user repeatability is diminished for lower quality offsets (Zielke and Arrowsmith, 2012). Uncertainties in measurements are based on maximum and minimum amounts of offset possible for a given feature, and they thus reflect a 95-percent confidence interval. Where possible we have validated each offset measurement made using the LiDAR data with those made in the field or on aerial photographs (see following section) or as part of published efforts by coauthors (San Jacinto Fault—Salisbury and others, 2012; 1857 reach of SAF—Zielke and others, 2012). The KML files for LiDAR measurements (supplementary file R1-2) include tabular data from the offset master data table (supplementary file R1-1) obtained using the offset analyses performed by the lateral displacement calculator (see, for example, Zielke and Arrowsmith, 2012).

Method Validation for New LiDAR Measurements

To test the first-order reliability of our LiDAR-derived slip measurements against their field counterparts, we compared the two datasets for the Garlock and San Jacinto Fault zones. Figure R3 shows the LiDAR- and field-derived offset measurements for the central section of the Garlock Fault plotted along strike. Qualitatively, both datasets show that LiDAR- and field-derived offset measurements yield similar along-strike offset distributions (supplementary file R2-2). Figures R4*A* and R4*B* show our LiDAR-derived slip measurements as a function of field measurements made for 129 offset features along the eastern section of the Garlock Fault and 125 offset features along the San Jacinto Fault zone. Offset measurements made in the field for the Garlock and San Jacinto Faults were compiled from McGill and Sieh (1991) and Salisbury and others (2012), respectively (supplementary file R1-1). Blue lines in figure R4 represent hypothetical perfect correlations between the field and LiDAR measurements. Our LiDAR-derived offsets compare well with the published field measurements, attaining a correlation coefficient R^2 of 0.9 for both fault zones. This validation demonstrates that, to a first order and for lateral displacements alone, LiDAR-derived measurements are reliable indicators of slip in the last few events and thus provide accurate representations of slip distributions for faults zones. J.B. Salisbury and coworkers are exploring offset validation further.

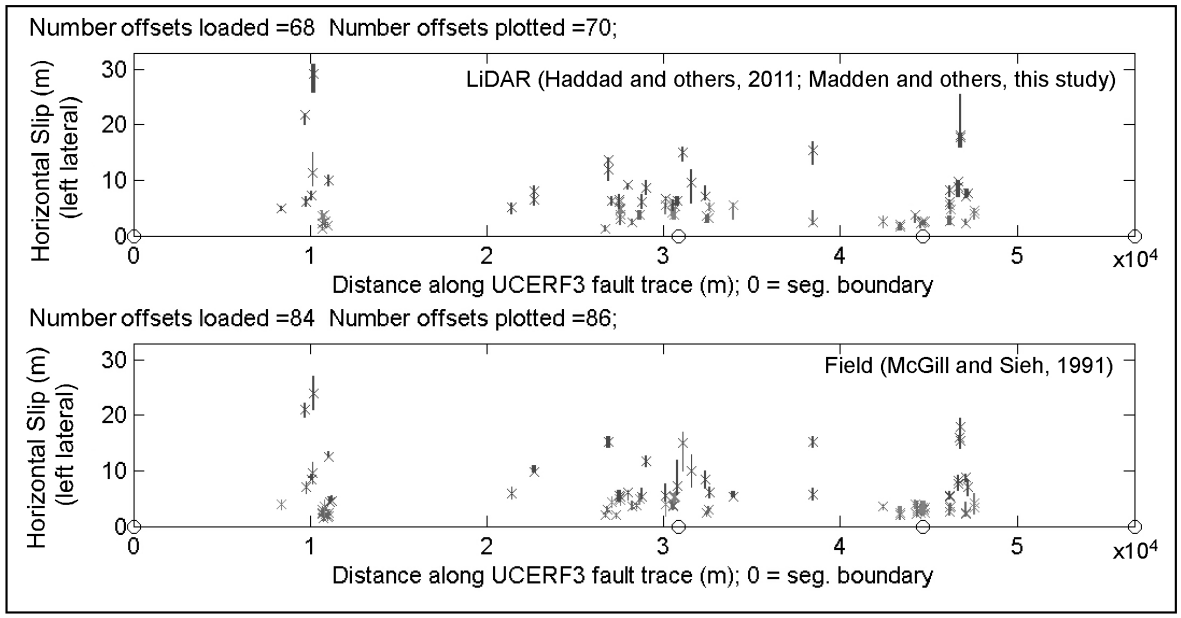

Figure R3. Plots showing qualitative comparison of LiDAR-derived (top) and field-derived (bottom) offset measurements for the central section of the Garlock Fault, plotted along strike.

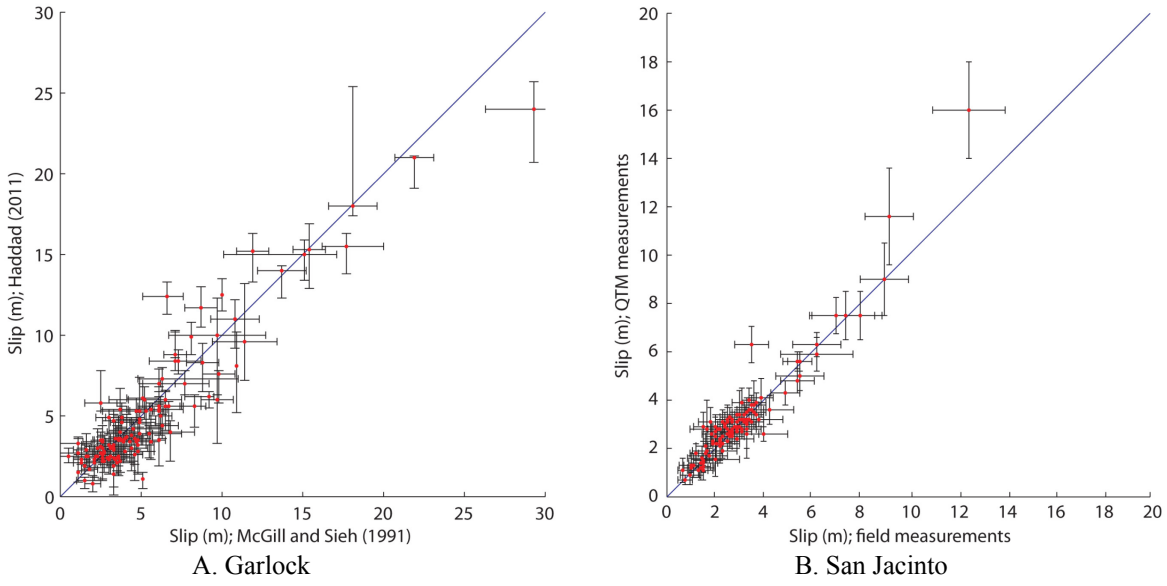

Figure R4. Graphs showing correlation of offsets measured from LiDAR with offset measurements made in the field along the same fault section. *A*, LiDAR and field measurements for the central Garlock Fault; *B*, LiDAR and field measurements from the Anza section of the San Jacinto Fault (Salisbury and others, 2012).

Offset Quality Rating Scheme

Measurement of offset features are typically made in the field (for example, Wallace, 1968; Sieh 1978; McGill and Sieh, 1991; Arrowsmith and Rhodes, 1994; McGill and Rubin, 1999; Lienkaemper, 2001) or using remote techniques (for exampole, Arrowsmith and Zielke, 2009; Zielke and others, 2010; Haddad and others, 2012; Klinger and others, 2011; Salisbury and

others, 2012; Zielke and others, 2012; and other works) and are often reported with a quality rating based on the investigators' confidence in the offset measurement as a reliable indicator of slip. However, because no standard rating scheme exists, existing reporting schemes for quality of slip measurements vary significantly and have a high degree of subjectivity. For this compilation we assign offsets to three quality categories: high, medium, and low (fig. R5). A rating of "high" represents offset measurements determined using clear fault-normal piercing lines that intersect a simple, well-defined fault zone. Conversely, a rating of "low" is assigned to measurements of features that are oblique to a broad, poorly defined fault zone. We assign "high" ratings to field measurements made in response to historical earthquakes and to paleoseismic studies where low-ambiguity slip measurements could be made.

To map existing rating schemes to our three-category UCERF3 scheme, we assign a rating of "high" to the highest quality measurements in other compilations and "low" to the lowest quality measurements. All other ratings receive a "medium" score (fig. R5). Supplementary file R3 summarizes existing quality rating schemes and introduces our proposed scheme that we used to standardize the quality assessment of our compiled slip measurements. A preliminary comparison between offset rating and measurement uncertainty reveals that high- and low-ranked offset features had the smallest and largest measurement uncertainties, respectively, with little effect on uncertainty for the intermediate quality ratings, regardless of how many intermediate ratings there were. Although beyond the scope of this report, additional work is required to test the sensitivity of displacement averages to quality ratings.

Sieh, 1978	*Lienkaemper, 2001*	*Zielke and others, 2010*	*UCERF 3*
Excellent	High	High	1
Excellent/Good		High-moderate	2
Good			2
Good/Fair	Medium	Moderate	2
Fair		Moderate-low	2
Fair/Poor			2
Poor	Low	Low	3

Figure R5. Tabular plot showing correlation of UCERF3 offset rating scheme to other published rating schemes.

Data Analysis

Characterizing Slip in Most Recent Earthquake

Given that most of the geomorphic offsets in our database have not been linked to a specific earthquake by postseismic field observations or paleoseismic data, we used two methodologies to characterize slip in the last event.

For the first method, local minimum geomorphic slip values along a given reach of the fault were assigned a ranking of "S", and offsets that could be tied directly to a historical earthquake rupture were assigned a ranking of "1" (for example, red in figure R6 and "S" and "1" in the number of events column in supplementary file R1-1). S values are not absolute minima, but rather encompass clusters of smaller offsets. Typically, these clusters of low offset values are separated from clusters of higher offset values. Rankings of "M" were given to slip values that likely were produced by more than one earthquake. Rankings of "S-M" were given to offsets that could represent single or multiple event offsets.

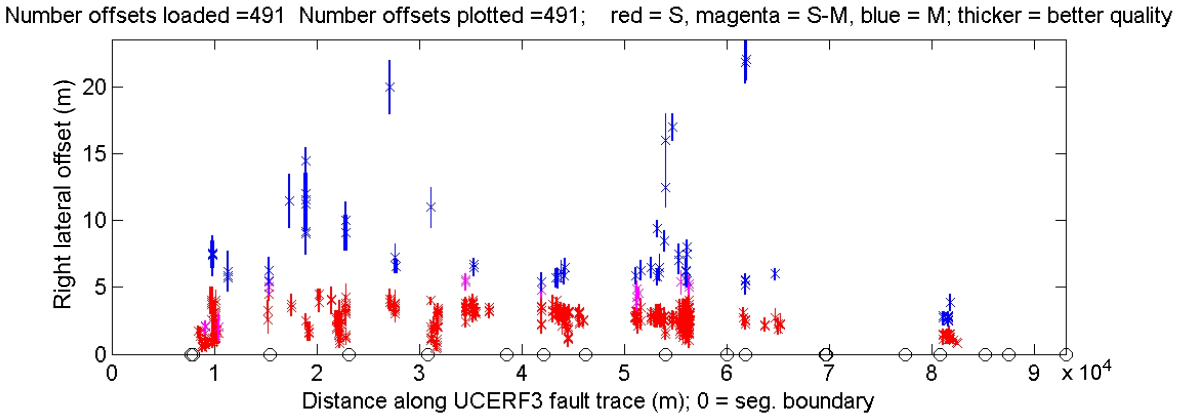

Figure R6. Plot of offsets along the Clark strand of the San Jacinto Fault coded for number of events and feature quality. Inferred single event offsets (S) are red, multievent offsets (M) are blue. Magenta is used to mark offsets where it is unclear whether they were formed from single or multiple events (S-M). The thickness of the uncertainty bars indicates the quality of the data; quality increases with line thickness.

More objectively, the second method consisted of a Cumulative Offset Probability Distribution (COPD) analysis that uses all measurements along a given reach of fault to generate a value for slip in the last event, which acts as a check on the mean of the S values. McGill and Sieh (1991) were early proponents of the COPD analysis approach. Each offset is represented as a triangular probability density function (PDF) with the peak at the offset or slip magnitude and the base spanning the +/- uncertainty about it. The triangle height is scaled by the UCERF3 quality rating score (1, 2, or 3). The COPD consists of the sum of individual PDFs for all of the offsets (not just the "S" values) across a specified offset range. Because the COPD is the sum of individual PDFs, its peak can exceed a value of one, whereas peaks of individual PDFs do not exceed a value of one. Figure R7 illustrates the construction of the COPD with the individual triangular PDFs (note their different heights indicating the different qualities) and the resulting sum (COPD) below.

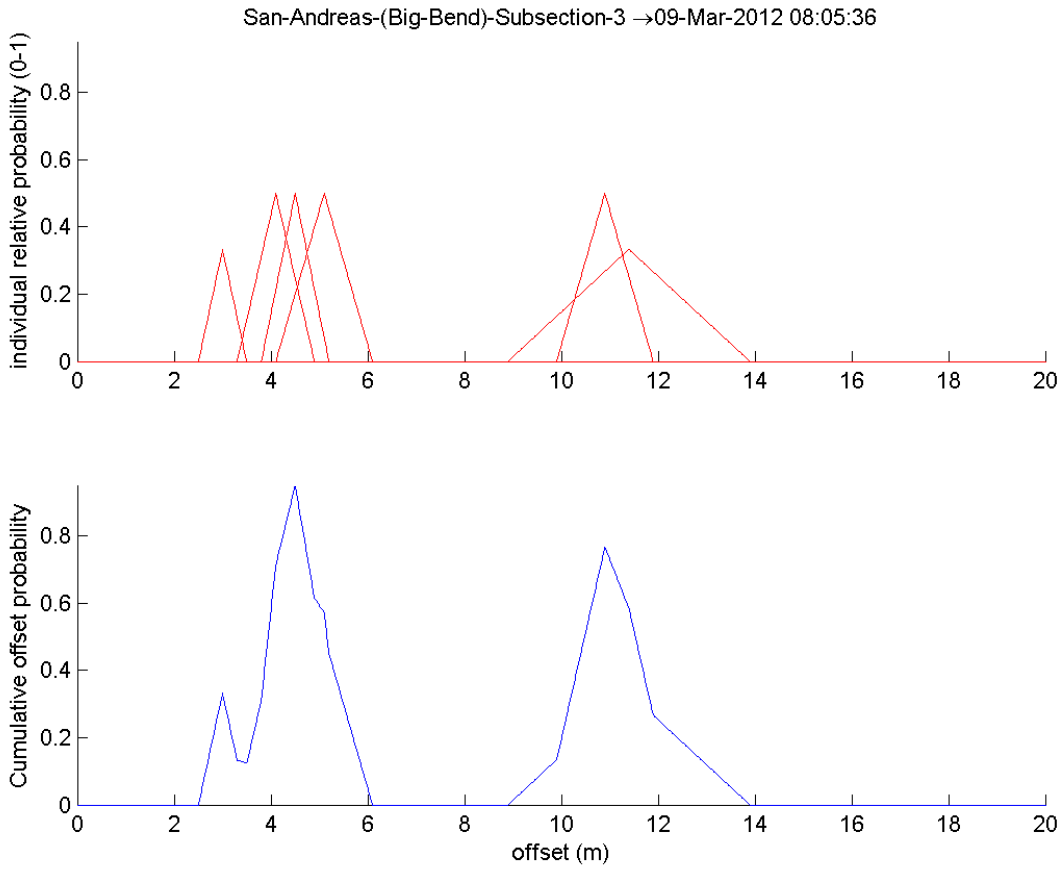

Figure R7. Plots showing cumulative offset probability distribution (COPD) for subsection 3 of the Big Bend section of the San Andreas Fault. This example shows how COPD curves are constructed from triangular offset measurement probability density functions (PDFs). The width of the base of the triangles in the upper plot reflects measurement uncertainty and the height of the triangle is scaled based on quality. The COPD represents the sum of the individual measurement PDFs. COPD max is 4.5 m.

We found that there is a tradeoff between longer fault reaches to draw from for the stacking (more measurements) and the problem that slip along the reach may not be constant and so the stacking becomes less meaningful (compare to figure R8 below—the entire Big Bend section—32 offsets—with COPD normalized and figure R7, which is just 6 offsets for the 7-km UCERF3 subsection). The latter problem is particularly evident for historical offset datasets (for example, McGill and Rubin, 1999).

For paleoseismic offset COPDs, we assume (like Wallace, 1968, and McGill and Sieh, 1991) that the largest COPD mode (COPD max) is associated with the lowest offset, and that this represents slip in the last event.

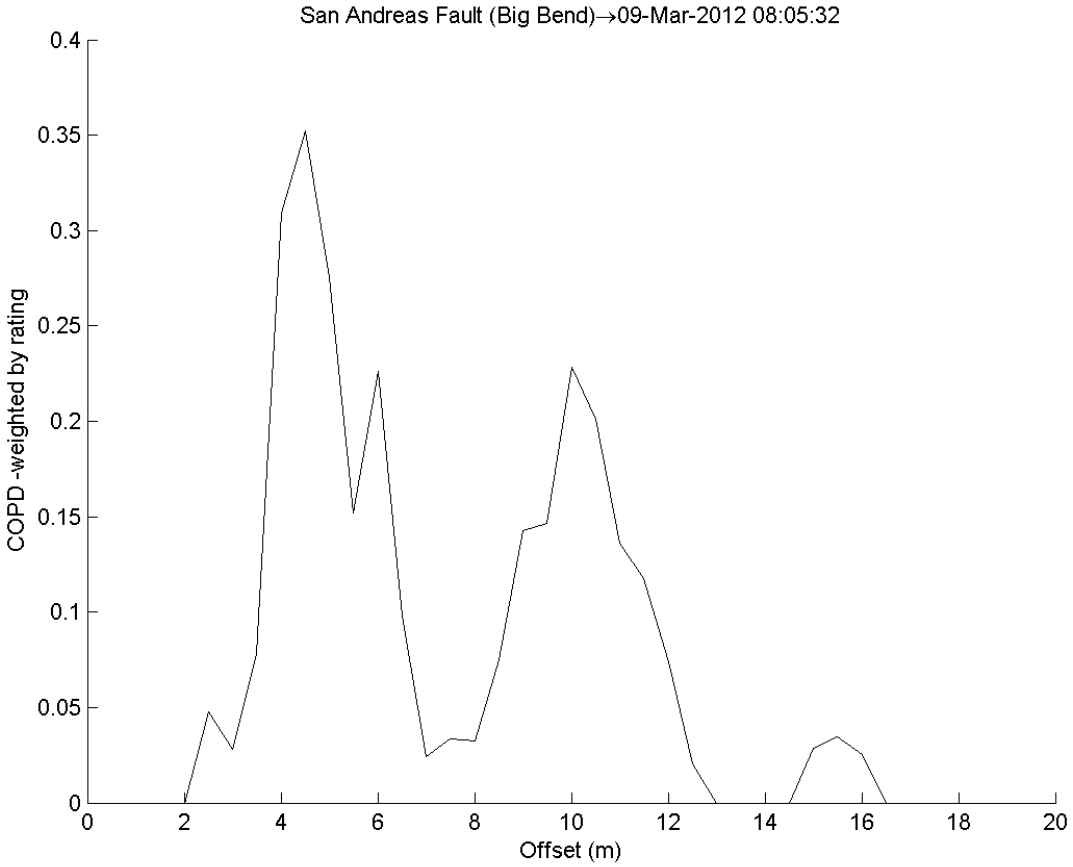

Figure R8. Graph showing normalized COPD for the entire Big Bend section of the San Andreas Fault. Compare with COPD for subsection 3 in figure R7.

Geometric Association of Offsets with UCERF3 Fault Subsections

The immediate use for our offset database is to provide direct information, where available, for the slip in the last earthquake along the ~7-km-long UCERF3 fault subsections (we used the 3.2 version of the fault database). Assigning specific offsets to their corresponding fault subsections enables their integration with other UCERF3 components. We summarized the offsets as single values for MRE slip with uncertainty and the COPD curve for each subsection. The subsection traces were straight and are simplified representations of the more complex fault zones along which the offsets were observed.

We systematically worked through the fault subsections and the offsets, starting first with the loose association by name from the database compilation. The coordinates for both the offset locations and the fault subsection ends and vertices are in latitude-longitude decimal degrees (typically 10^{-6} precision). The coordinates were projected to UTM meters (using the Geodetic toolbox in MATLAB: *http://www.mathworks.com/matlabcentral/fileexchange/15285*). A 1-km-wide across-strike buffer was defined along each fault section or subsection. All offsets located in the buffer were orthogonally projected to the corresponding fault subsection (fig. R9). Cumulative distance along the fault section or subsection was then used as a measure of relative position for the subsequent computations.

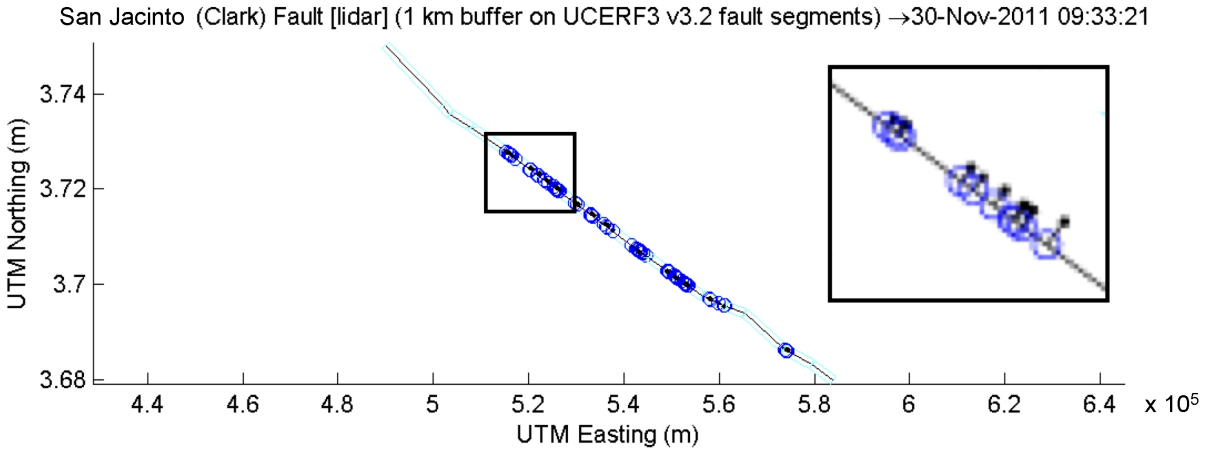

Figure R9. Graph of offset measurements projected orthogonally onto a UCERF 3.2 fault element. Projected offsets limited to a 1-km buffer on either side of the fault element (blue box).

Assigning Slip in Most Recent Earthquake to the UCERF3 Subsections

Based on the methodology described above in the section on "Characterizing Slip in Most Recent Earthquake," we computed two sets of measures for MRE slip for each subsection along which there was at least one measured offset inferred to represent a single earthquake: (1) the mean and the standard deviation of the inferred single event offsets ("S" or "1") and (2) the maximum cumulative offset probability distribution (COPD max). We calculated the mean and standard deviation for S values only. All MRE slip values derived from maximum COPD peaks were reviewed to evaluate whether offsets were reasonable. For older historical or prehistoric offsets, we deemed the agreement of mean S values and COPD max for a subsection to be of the highest quality. For subsections where the average and COPD disagreed, we chose a preferred value based on nearby paleoseismic data, high-quality MRE slip values from adjacent subsections, or our judgment of which value best represents MRE slip (fig. R10).

For offsets that can be indisputably tied to slip in the last event—measurements made immediately after a rupture, for example—we calculated the mean of all offsets along a subsection and the COPD max, and we identified the maximum slip and highest COPD peak. In this case the maximum COPD mode is a minimum slip value that accounts for offset from only the most significant fault strand on a subsection and does not take into account deformation along secondary fault strands. If the fault is straight, we interpreted the maximum slip for the subsection to be the closest representation of slip for the entire fault plane, especially if the maximum slip was in agreement with the highest COPD curve.

MATLAB scripts and functions used to run these analyses are included in supplementary files R4. Input files derived from our offset database (supplementary file R1-1) are included in supplementary files R4-1 to R4-5.

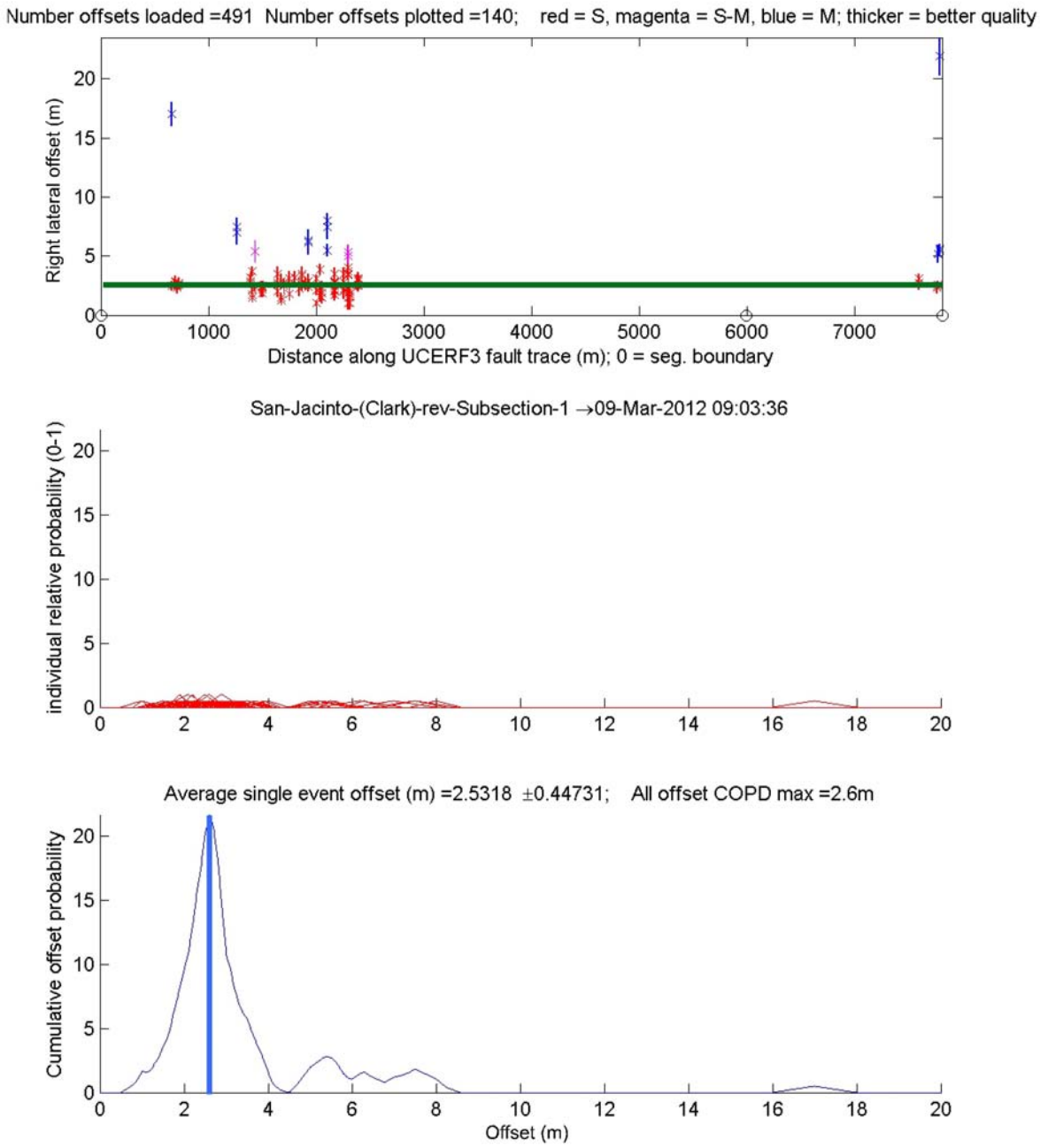

Figure R10. Graphical plots showing comparison of the mean of S measurements (green line in top panel) and COPD max (blue line in bottom panel) for 140 offsets on subsection 1 of the Clark strand of the San Jacinto Fault. Middle panel shows triangular probability distribution functions derived from offset measurements used to calculated cumulative offset probability distribution (COPD) in the lower panel. We consider the close agreement of the offsets derived using these two methods a robust constraint on slip in the last event.

Estimating Repeated Slip for Selected UCERF3 Subsections and Points

For subsections with multiple distinctive COPD peaks, we determined repeated slip per event for a subsection by measuring the distance between the highest COPD modes (fig. R11; supplementary files R7). This analysis was limited to subsections with clear COPD peaks,

defined in most cases by at least three offsets. We infer that each clear COPD mode represents cumulative slip from a number of events, which is equivalent to the number of COPD modes. Thus, we assume that the distance between any two peaks represents slip from one event. We assigned an uncertainty to these measurements equivalent to the half-width of the COPD mode. To characterize average slip per event, we calculated the weighted mean of the slip measurements for each subsection. We also calculated average slip per event at a point for several paleoseismic datasets included in our database (for example, Leon and others, 2007, 2009; Liu and others, 2004; Liu-Zeng and others, 2006).

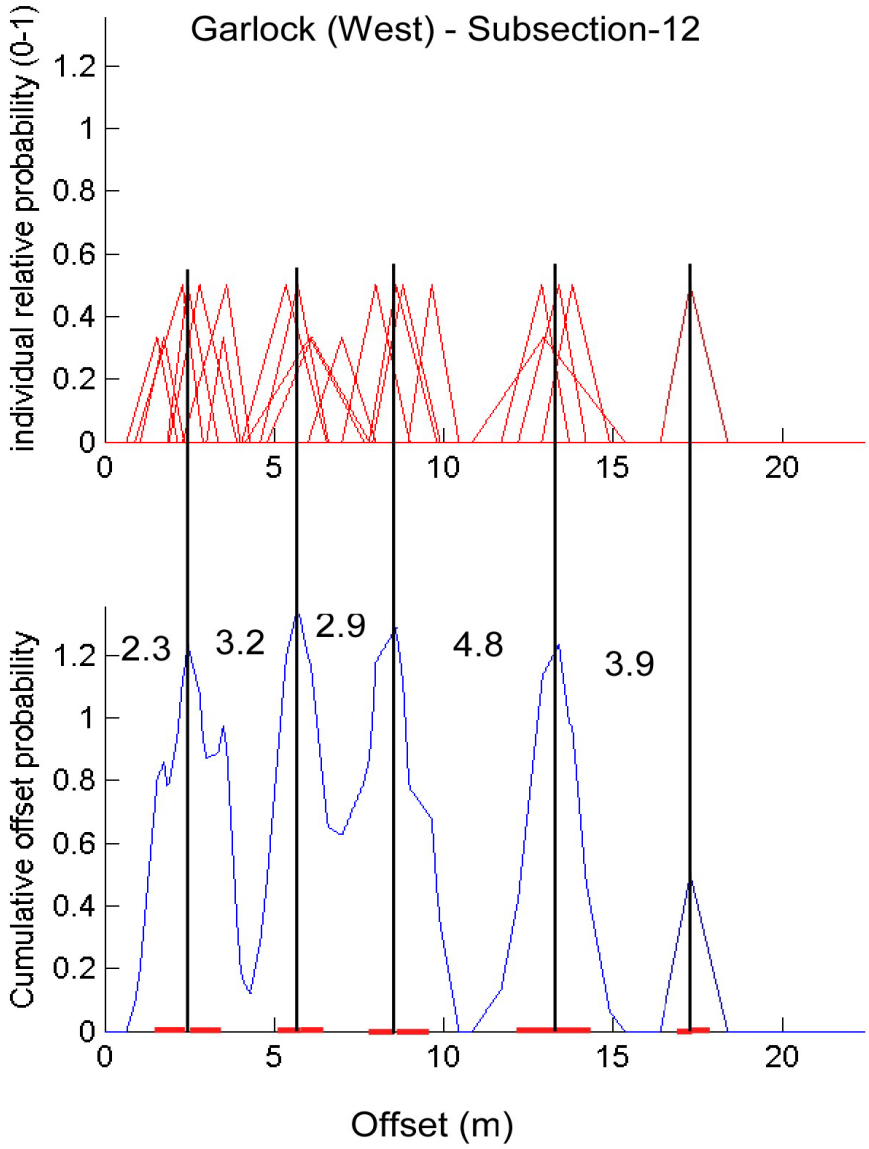

Figure R11. Graphs showing estimate of repeated slip for subsection 12 of the western Garlock Fault determined by measuring the distance between cumulative offset probability distribution (COPD) peaks. Upper panel shows triangular probability distribution functions derived from offset data and lower panel shows COPDs calculated from the probability distribution functions in the upper panel. Error bars (red) in the lower panel are defined by half of the width of each curve.

Calculating Average Displacement for Older Historical and Prehistoric Ruptures

We calculated average displacement by taking the mean of S measurements and associated uncertainty for the given reach of the fault that ruptured based on paleoseismology or abrupt slip gradients.

Results

The results of our analyses are presented in tables R3–R7 at the end of this appendix. For subsections where different analyses are not in agreement, we highlight a preferred value. Raw output files from the MATLAB scripts and figures showing distribution of S, S–M, and M offsets, COPD curves, and repeated slip measurements are compiled in supplementary files R6-1 to R6-4.

Slip in the Last Event

Recent Historical Ruptures

In the context of this report, "recent historical" refers to all historical ruptures that were followed by a dedicated field-mapping program to measure offsets. Slip in the last event for recent historical ruptures encompasses 60 subsections. All but three subsections include more than one measurement. Table R3 compiles average slip measurements for each subsection derived using the methods described above, and table R4 compiles our best estimates for slip in the last event for each subsection.

Assuming no significant afterslip occurred, we believe that the maximum slip for each subsection is the best approximation of slip at depth and provides the best input for time-dependent rupture models. The maximum slip and highest distinctive COPD peak are within error for 12 subsections and within a factor of two for an additional 15 subsections. We interpret this agreement as a robust indicator that these values represent slip at depth. It is important to note, however, that for smaller ruptures, the maximum slip is still less than slip at depth. Additional work should be done to correlate how dependent this agreement is on fault complexity and how well these values correlate to inversions of slip at depth.

Older Historical and Prehistoric Ruptures

For this report, "older historical and prehistoric" refers to ruptures in which slip in the last event was not observed immediately following the event using offset topography (landforms) or subsurface contacts (for example, buried channel boundaries). Slip in the last event for older historical and prehistoric ruptures encompasses 98 subsections (tables R5 and R6). Nearly a third of these subsections (30 subsections) contain only one inferred-slip measurement. S and COPD max are similar for 19 of these 30 subsections.

The mean of the S-coded measurements and the COPD max were within error in half of the subsections with more than one measurement (34 of 68 subsections) and within a factor of two in an additional 20 subsections. We interpret the strong correlation of mean S and COPD max as a robust indicator that these values represent slip in the last event. For 10 subsections, the mean S and COPD max values were off by more than a factor of two. Where the values do not agree, we offer a best estimate based on evaluation of the COPD curve, quality of measurements, and slip on adjacent fault subsections.

Several factors may explain the disagreement between mean S and COPD max. For subsections with only one S measurement, disagreement between S and COPD max has two possible causes. The inclusion of multi-slip values into the COPD max would overestimate slip for the last event. Conversely, the S measurement could be a minimum value for slip in the last event.

For subsections with multiple S measurements, disagreement between mean S and COPD max could be due to poor constraints on slip due to low measurement quality, localized low slip values due to structural complexities or segment boundaries, poorly defined COPD peaks due to along-strike variations in slip, and skewed COPD peaks due to weighting by high-quality measurements. Some of these issues are discussed further in the "Discussion" section, below.

Repeated Slip

COPD Curves

Offset measurements made along 17 subsections of the San Andreas, Elsinore, Garlock, and San Jacinto Faults produced two to five strong COPD peaks (table R7). Based on the assumption that each distinctive peak represents cumulative slip for an event plus slip from all previous events and the distance between the peaks represents slip for an individual event, we graphically calculated repeated slip for each subsection. After normalizing the offsets to the mean, we determined that the coefficient of variation was typically low (significantly less than 1), possibly suggesting characteristic displacement for a subsection.

Paleoseismology

Table R8 shows repeated slip at a point from paleoseismic data for the Puente Hills, Compton, and San Andreas Faults. The sites along the San Andreas include Wallace Creek, Wrightwood, and Pallet Creek. Slip at each of these sites appeared quite characteristic.

Average Displacement

Table R9 shows average displacement for events on the Garlock (A.D. 1450–1640), Owens Valley (1872), San Jacinto (1880, 1550), and San Andreas (1690, 1857) Faults. Rupture endpoints were based on published data or rapid decreases in offsets.

Discussion

Variations in COPD: What Do Peaks Actually Represent?

For paleoseismic offset COPDs, we assume (like Wallace, 1968, and McGill and Sieh, 1991) that the largest COPD mode (COPD max) is associated with the smallest offset. As the offset increases, COPD modes decrease in height precipitously. Klinger and others (2011) and Zielke and others (2012) use the decay of the COPD peak height as a gross measure of the geomorphic preservation of the offset features (fig. R12).

For geomorphic offsets from older historical or prehistoric events, some peaks have shoulders or second humps which may or may not represent additional events. This leads to the general question for the COPDs of what relative height of a peak is great enough to be significant (fig. R12*A*, mode at 3–6 m with multiple subpeaks)? This question may be answered

partially by exploring the recent historical offsets (Landers, Hector Mine, Superstition Hills). In these historical cases, where we know that all offsets are from a single earthquake, the multiple humps clearly show that the largest peak is the more coherent slip and the smaller peaks correlate to slip that is more distributed.

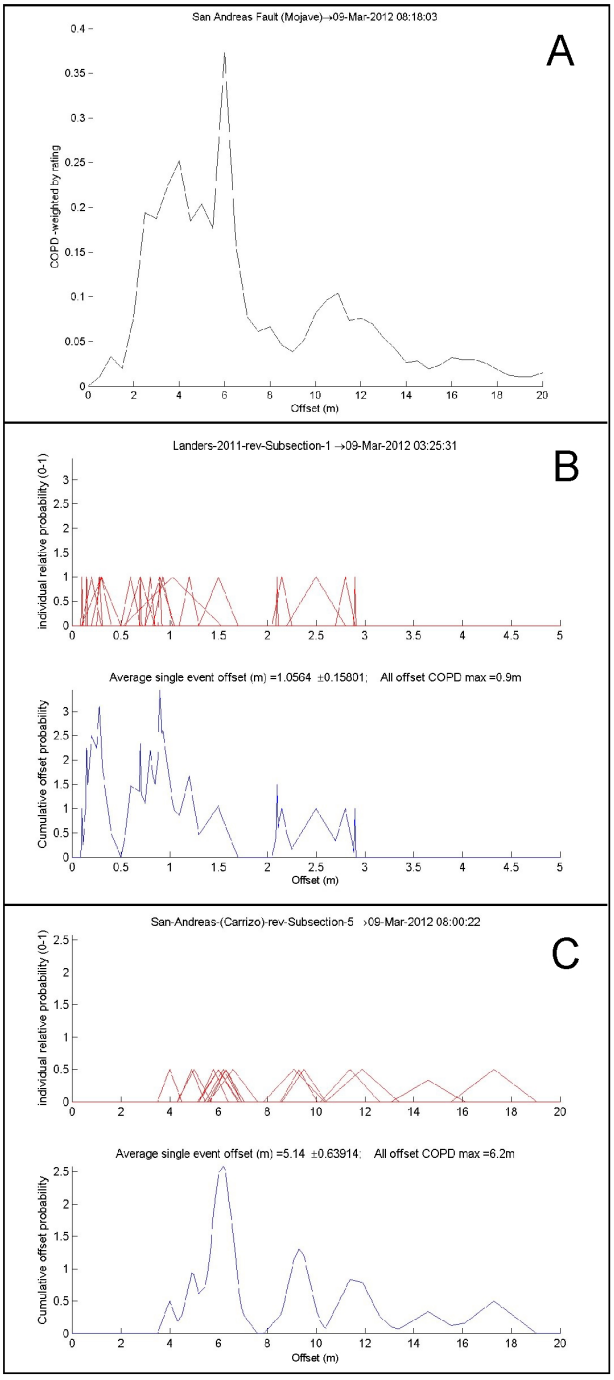

Figure R12. Plots showing exploration of subpeaks on main cumulative offset probability distribution (COPD) peaks. *A*, COPD mode between 3 and 6 m has multiple subpeaks. Do these subpeaks represent multiple events? *B*, COPD peaks calculated using field measurements from a single rupture. Highest peaks likely represent slip on main fault strands, and subpeaks likely represent slip on secondary faults. *C*, COPD calculated using geomorphic offsets that likely represent multiple ruptures. Strongest peaks likely represent slip on the main fault strand during five individual events. Subpeaks on the COPD max are residual smaller offsets from secondary fault strands. Higher COPD peaks do not have subpeaks because smaller offsets have not been preserved geomorphically.

This inference for recent historical ruptures is opposite to our interpretations of multiple event sequences where the minimum offset peak is the MRE. We suggest that there is an evolution in COPD peaks over the time following a surface rupture; a given event produces a multi-humped COPD where the larger offset peak represents slip on a primary fault strand and subpeaks represent distributed slip on secondary fault strands (fig. R12*B*).

Over time the small offsets are eroded away, or covered by deposition, and can no longer be identified in the field or from LiDAR data. The largest geomorphic offsets that are preserved thus likely represent slip on the main fault strand, and increasing offsets represent slip from multiple events. In this way the complex individual event COPDs come together in the multi-event COPD with the declining preservation tail to longer offsets (fig. R12*C*).

COPD peaks can also be muted when there is no clear cluster of offset magnitudes. We found this smearing was evident in cases in which there was significant along-strike variation in MRE slip (especially recent historical earthquakes; figure R13 shows this for the Homestead Valley Fault subsection 4 for the 1992 Landers earthquake offsets) or in MRE classification.

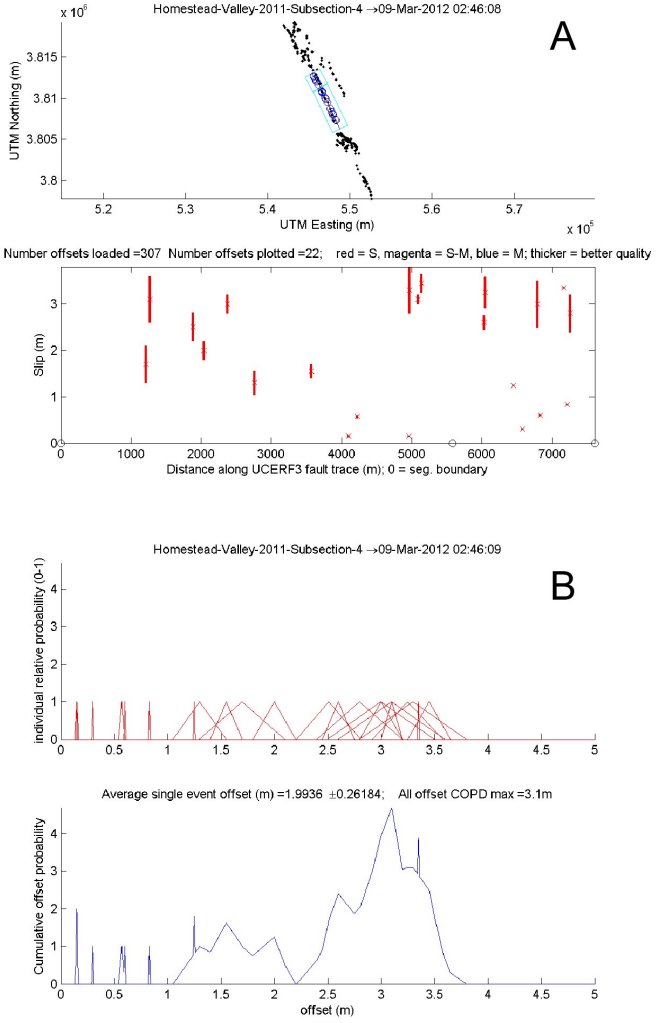

Figure R13. *A*, Map of UCERF subsection 4 of the Homestead Valley Fault (upper panel) and offsets measured on this part of the fault after the 1992 Landers earthquake (lower panel). Measurement uncertainties are shown as vertical bars. *B*, Plot with offsets measurements and associated uncertainties from A shown as triangular PDFs (upper panel). Cumulative offset probability distribution (COPD) for the PDFs shows a smeared peak between 1 m and 2 m (lower panel).

Broader Implications

Looking at the entire database provides important slip-per-event constraints for California (fig. R14). The upper panel of figure R14 shows single-event offsets binned by number of measurements per slip value. The small offsets between 0 and 1 m come primarily from recent historical *M*6–7.3 events and another mode around 2–3 m comes from larger historical events. We see typical offsets of 3–5 m along the SAF and 2–3 m from prehistoric events on other large faults such as the Garlock and San Jacinto Faults. The maximum slip that can be attributed to a single-event offset is 7.9 m. This value is an outlier, however, and all other offsets fall below 6.3 m. Based on our analysis, we typically do not see the larger displacements predicted by some magnitude or average displacement scaling relationships. The lower panel of figure R14 shows the histogram of minimum offset (but highest) COPD peaks for each UCERF3 subsection. Here, we find that some reaches have strong peaks at higher offset, but these peaks probably reflect more than one offset along that reach, given that in most cases, lower peaks are evident at smaller offset.

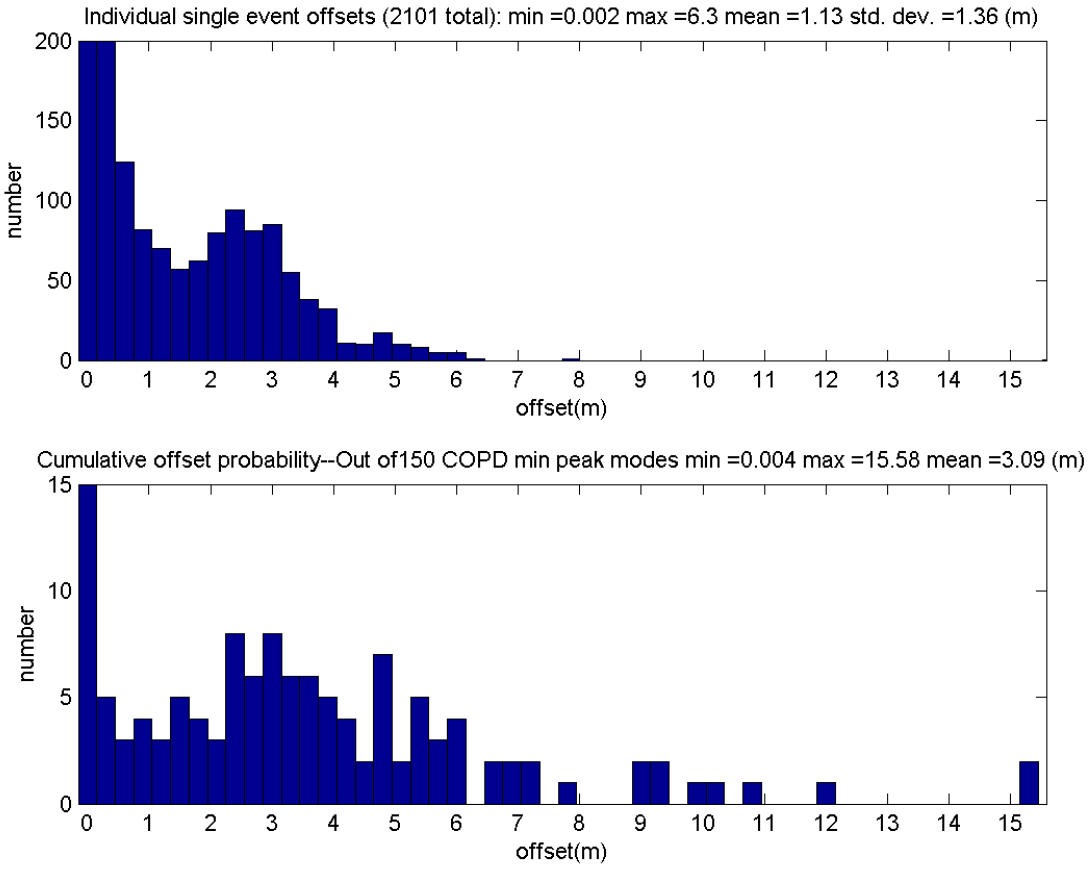

Figure R14. Histograms of all offsets in the database. Upper panel, individual single-event offsets; lower panel, cumulative offset probability. Note distinctive modes between 0 and 1 m, 2.5–3.5 m, and ~ 5 m.

Conclusion

This work represents the most comprehensive database of slip measurements for high-slip-rate strike-slip and dip-slip faults in California to date for input into the time-dependent Uniform California Earthquake Rupture Forecast, version 3. Our primary conclusions are as follows:

4. Our compilation includes 2,101 measurements for slip in the last event and inferred slip in the last event. Small offsets between 0 and 1 m come primarily from recent historical *M*6–7.3 events, and another mode around 2–3 m comes from larger historical events (fig. R1).
5. We see typical offsets of 3–5 m on the SAF and 2–3 m from prehistoric events on other large faults such as the Garlock and San Jacinto Faults. With one exception, all single-event offsets and inferred singe-event offsets fall below 6.3 m. We therefor do not see the very large displacements predicted by some scaling relationships.
6. More than 17 subsections have several COPD peaks that can be used to infer average slip per event.
7. We have identified six discrete ruptures on the San Andreas, Garlock, San Jacinto, and Owens Valley Faults in which we can constrain rupture end points based on abrupt decreases in geomorphic offset and existing paleoseismic data. These ruptures have enough displacement measurements between their end points to calculate average displacement per event. These data can provide support for the California-only scaling relations between length and average displacement being proposed as a possible model.

Acknowledgements

We are grateful to the many people and organizations that contributed time, data, and financial support to this compilation effort. J. Baldwin, T. Dawson, J. Dolan, N. Field, P. Ganev, E. Gath, T. Gonzalez, K. Kelson, J. Lienkaemper, D. Madugo, S. McGill, K. Milner, M. Oskin, C. Prentice, S. Ramzan, T. Rockwell, T. Sato, D. Schwartz, M. Strane, G. Seitz, A. Streig, S. Thompson, J. Treiman, C. Walls, P. Williams, D. Yule, and many others contributed data, observations, interpretation and time to this effort. K. Scharer and W. Lettis provided useful reviews that significantly improved this appendix. Thanks to T. Sato and L. Weldon for compiling references. Additional data and financial support was provided by the Working Group on California Earthquake Probabilities, the California Earthquake Authority, the Southern California Earthquake Center, the United States Geological Survey, the California Geological Survey, the National Earthquake Hazards Reduction Program, and Open Topography (www.OpenTopography.org).

The EarthScope LiDAR acquistion was based on services provided to the Plate Boundary Observatory (PBO) by NCALM (*http://www.ncalm.org*). PBO is operated by UNAVCO for EarthScope (*http://www.earthscope.org*) and supported by the National Science Foundation (No. EAR-0350028 and EAR-0732947). *http://dx.doi.org/10.5069/G9G44N6Q*

Processing services provided by the OpenTopography Facility with support from the National Science Foundation under NSF Award Numbers 0930731 and 0930643.

References

Akciz, S.O., Grant, L.L., Arrowsmith, J.R., and Zielke, O., 2010, Century-long average time intervals between ruptures of the San Andreas fault in the Carrizo Plain: Geology, v. 38, p. 787–790, doi:10.1130G30995.1.

Arrowsmith, J.R., and Rhodes, D.D., 1994, Original forms and initial modifications of the Galway Lake road scarp formed along the Emerson fault during the 28 June 1992 Landers, California earthquake: Seismological Society of America Bulletin, v. 84, p. 511–527.

Arrowsmith, J.R., and Zielke, O., 2009, Tectonic geomorphology of the San Andreas fault zone from high-resolution topography—an example from the Cholame segment: Geomorphology, v. 113, p. 70–81.

Arrowsmith, J.R., Madden, C., Haddad, D.E., Salisbury, J.B., and Weldon, R.J., 2011, Compilation of slip in last earthquake data for high-slip rate faults in California for input into slip dependent rupture forecast [abs]: American Geophysical Union, Fall meeting 2011, abstract S13B-06.

Baldwin, J.N., 1996, Paleoseismic investigation of the San Andreas fault on the north coast segment, near Manchester, California: San Jose State University, MS thesis, 127 p.

Baldwin, J.N., and Lienkaemper, J.J., 1999, Paleoseismic investigations along the Green Valley fault, Solano County, California: Bay Area Paleoseismological Experiment Contract, Unpublished report 98WRCN1012, 18 p.

Baldwin, J.N., Knudsen, K.L., Lee, A., Prentice, C.S., and Gross, R., 2000, Preliminary estimate of coseismic displacement of the penultimate earthquake on the northern San Andreas fault, Pt. Arena, California in Bokelman G., and Kovachs R., eds., Tectonic Problems of the San Andreas Fault System: Stanford University Publications, Geological Sciences, v. 21, p. 355–368.

Barrows, A.G., Kahle, J.E., Weber, F.H., Jr., and Saul, R.B., 1973, Map of surface breaks resulting from the San Fernando, California, earthquake of February 9, 1971, in San Fernando, California, earthquake of February 9, 1971: Washington, D.C., National Oceanic and Atmospheric Administration, v. 3, p. 127–135.

Beanland, S., and Clark, M.M., 1994, The Owens Valley fault zone, eastern California, and surface rupture associated with the 1872 earthquake: U.S. Geological Survey Bulletin 1982, 29 p.

Biasi, G.P., and Weldon, R.J., II, 2006, Estimating surface rupture length and magnitude of paleoearthquakes from point measurements of rupture displacement: Seismological Society of America Bulletin, v. 96, p. 1612–1623.

Budding, K.E., Schwartz, D.P., and Oppenheimer, D.H., 1991, Slip rate, earthquake recurrence, and seismogenic potential of the Rodgers Creek fault zone, northern California—Initial results: Geophysical Research Letters, v. 18, no. 3, p. 447–450.

Carver, G.A., and Burke, R.M., 1988, Trenching investigations of northwestern California faults, Humboldt Bay region: U.S. Geological Survey, National Earthquake Hazards Reduction Program, Final Technical Report, 53 p.

Clark, M.M., 1972, Surface rupture along the Coyote Creek fault, the Borrego mountain earthquake of April 9, 1968: U.S. Geological Survey Professional Paper 787, p. 55–86.

Dolan, J.F., and Rockwell, T.K., 2001, Paleoseismologic evidence for a very large (Mw>7), post-A.D. 1660 surface rupture on the eastern San Cayetano fault, Ventura County, California—was this the elusive source of the damaging 21 December 1812 earthquake?: Seismological Society of America Bulletin, v. 91, p. 1417–1432.

Dolan, J.F., Bowman, D.D., and Sammis, C.G., 2007, Long-range and long-term fault interactions in southern California: Geology, v. 35, p. 855–858.

Field, E.H., and Page, M.T., 2011, Estimating earthquake-rupture rates on a fault or fault system: Seismological Society America Bulletin, v. 101, doi:10.1785/0120100004.

Frankel, K.L., Dolan, J.F., Owen, L.A., Finkel, R.C., and Hoeft, J.S., 2007, Spatial variations in slip rate along the Death Valley-Fish Lake Valley fault system from LiDAR topographic data and cosmogenic Be chronology: Geophysical Research Letters, v. 34, doi:1029/2006JB004350.

Fumal, T.E., Heingartner, G.F., and Schwartz, D.P., 1999, Timing and slip of large earthquakes on the San Andreas fault, Santa Cruz mountains, California [abs]: Geological Society of America Abstracts with Programs, v. 31, no. 6, p. A-56.

Ganev, P.N., Dolan, J.F., Blisniuk, K., Oskin, M., and Owen, L., 2010, Paleoseismic evidence for multiple Holocene earthquakes on the Calico fault—implications for earthquake clustering in the eastern California shear zone: Lithosphere, v. 2, p. 287–298, doi:10.1130/L82.1.

Gath, E.M., Gonzalez, T., and Rockwell, T.K., 1992, Slip rate of the Whittier fault based on 3-D trenching at Brea, southern California [abs.]: Geological Society of America Abstracts with Programs, v. 24, no. 5, p. 26.

Gonzalez, T., and Rockwell, T.K., 1991, Holocene Activity of the Springville Fault in Camarillo, Transverse Ranges, Southern California; Preliminary Observations *in* Blake, T.F. and Larson, R.A. (eds.), Engineering Geology along the Simi-Santa Rosa Fault System and Adjacent Areas, Simi Valley to Camarillo, Ventura County, California; Field Trip Guidebook of the 1991 Annual Field Trip, Southern California Section: Association of Engineering Geologists, p. 369–383.

Grant-Ludwig, L.B., Akçiz, S.O., Noriega, G.R., Zielke, O., and Arrowsmith, J.R., 2010, Climate-modulated channel incision and rupture history of the San Andreas fault in the Carrizo Plain: Science, v. 327, p. 1117–1119, doi:10.1126/science.1182837.

Green, A., Gross, R., Holliger, K., Horstmeyer, H., and Baldwin, J., 2003, Results of 3-D georadar surveying and trenching the San Andreas fault near its northern landward limit: Tectonophysics, v. 368, no. 1, p. 7–23.

Haddad, D.E., Akçiz, S.O., Arrowsmith, J.R., Rhodes, D.D., Oldow, J.S., Zielke, O., Toké, N.A., Haddad, A.G., Mauer, J., and Shilpakar, P., 2012, Applications of airborne and terrestrial laser scanning to paleoseismology, *in* Seeing the true shape of Earth's surface—applications of airborne and terrestrial LiDAR in the geosciences, themed issue: Geosphere, v. 8, p. 1–16.

Haddad, D.E., Madden, C., Salisbury, J.B., Arrowsmith, J.R., and Weldon, R.J, 2011, LiDAR derived measurements of slip in the most recent ground-rupturing earthquakes along elements of the San Andreas fault system [abs]: Eos (American Geophysical Union Transactions), v. 92, Fall meeting supplement, abstract T31B-2344.

Hall, N.T., Wright, R.H., and Clahan, K.B., 1999, Paleoseismic studies of the San Francisco Peninsula segment of the San Andreas fault zone near Woodside, California: Journal of Geophysical Research (Solid Earth), v. 104, no. B10, p. 23215–23236.

Hecker, S., Pantosti, D., Schwartz, D.P., Hamilton, J.C., Reidy, L.M., and Powers, T.J., 2005, The most recent large earthquake on the Rodgers Creek fault, San Francisco Bay Area: Bulletin of the Seismological Society of America, v. 95, no. 3, p. 844–860.

Hemphill-Haley, M.A., and Witter, R.C., 2004, Latest Pleistocene paleoseismology of the southern Little Salmon fault, Strong's Creek, Fortuna, California: U.S. Geological Survey, National Earthquake Hazards Reduction Program, Final Technical Report, 19 p.

Hudnut, K., Borsa, A., Glennie, C., and Minster, J.B., 2002, High-resolution topography along surface rupture of the 16 October 1999 Hector Mine, California, earthquake (Mw7.1) from airborne laser swath mapping: Seismological Society of America Bulletin, v. 92, p. 1570–1576.

Kelson, K.I., Streig, A.R., Koehler, R.D., and Kang, K.H., 2006, Timing of late Holocene paleoearthquakes on the northern San Andreas fault at the Fort Ross orchard site, Sonoma County, California: Seismological Society of America Bulletin, v. 96, p. 1012–1028.

Klinger, Y., Etchebes, M., Tapponnier, P., and Narteau, C., 2011, Characteristic slip for five great earthquakes along the Fuyun fault in China: Nature Geoscience, v. 4, p. 389–392, doi:10.1038/NGEO1158.

Lawson, A.C., 1908, The California earthquake of April 18, 1906—Report of the state earthquake investigation commission: Washington, D.C., Carnegie Institution of Washington Publication 87.

Leon, L.A., Christofferson, S.A., Dolan, J.F., Shaw, J.H., and Pratt, T.L., 2007, Earthquake-by-earthquake fold growth above the Puente Hills blind thrust fault, Los Angeles, California—implications for fold kinematics and seismic hazard: Journal of Geophysical Research, v. 112, p. B03S03, doi:10.1029/2006JB004461.

Leon, L.A., Dolan, J.F., Shaw, J.H., and Pratt, T.L., 2009, Evidence for large-magnitude Holocene earthquakes on the Compton blind thrust fault, Los Angeles, California: Journal of Geophysical Research, v. 114, no. B12305, doi:10.1029/2008JB006129.

Lienkaemper, J.J., 2001, 1857 slip on the San Andreas fault southeast of Cholame, California: Seismological Society of America Bulletin, v. 91, p. 1659–1672.

Liu, J, Klinger, Y., Sieh, K., and Rubin, C. 2004, Six Similar sequential ruptures of the San Andreas fault, Carrizo Plain, California, Geology v. 32 no. 8 p. 649-652.

Liu-Zeng, J., Klinger, Y., Sieh, K., Rubin, C., and Seitz, G., 2006, Serial ruptures of the San Andreas fault, Carrizo Plain, California, revealed by three-dimensional excavations [abs.]: Journal of Geophysical Research (Solid Earth), v. 111, no. B2, doi: 10.1029/2004JB003601.

Madden, C.L., Arrowsmith, J.R., Haddad, D.E., Salisbury, J.B., and Weldon, R.J., 2011, Compilation of slip in the last earthquake data for high-slip rate faults in California for input into slip dependent rupture forecast [abs]: Southern California Earthquake Center Annual Meeting Proceedings and Abstracts, v. 21.

McAuliffe , L.M., Dolan, J.F., Kirby, E., Haravitch, B., and Alm, S., 2010, Holocene Paleoseismology of the southern Panamint Valley fault zone—evaluating seismic clustering along the eastern California shear zone north of the Garlock fault: Southern California Earthquake Center Annual Meeting Proceedings and Abstracts, v. 21, p. 249.

McCalpin, J.P., 2009, Paleoseismology (2d ed.): San Diego, Academic Press, International Geophysics Series, v. 95, 848 p.

McGill, S.F., and Rubin, C.M., 1999, Surficial slip distribution on the central Emerson fault during the June 28, 1992, Landers earthquake, California: Journal of Geophysical Research, v. 104, no. B3, p. 4811–4833.

McGill, S.F., and Sieh, K., 1991, Surficial offsets on the central and eastern Garlock fault associated with prehistoric earthquakes: Journal of Geophysical Research, v. 96, no. 21, p. 21597–21621.

Oskin, M.E., Lee, K., and Strane, M.D., 2007, Quantifying fault-zone activity in arid environments with high-resolution topography: Geophysical Research Letters, v. 34 no. 23, doi:10.1029/2007GL031295.

Oswald, J.A., and Wesnousky, S.G., 2002, Neotectonics and Quaternary geology of the Hunter Mountain fault zone and Saline Valley region, southeastern California: Geomorphology, v. 42, p. 255–278.

Padgett, D.C., 1994, Paleoseismology of the Lenwood fault, Mojave Desert, San Bernardino County, California: Los Angeles, California State University, M.S. thesis, 90 p.

Patterson, A.C., and Rockwell, T.K., 1993, Paleoseismology of the Whittier fault based on 3-dimensional trenching at Olinda oil field, Orange County, southern California [abs.]: Geological Society of America Abstracts with Programs, v. 25, no. 5, p. 131.

Peterson, M.D., Dawson, T.E., Chen, R., Tianqing, C., Wills, C.J., Schwarz, D.P., and Frankel, A.D., 2011, Fault displacement hazard for strike-slip faults: Seismological Society of America Bulletin, v. 101, p. 805–825, doi:10.1785/0120100035.

Prentice, C.S., and Ponti, D.J., 1997, Coseismic deformation of the Wrights tunnel during the 1906 San Francisco earthquake—a key to understanding 1906 fault slip and 1989 surface ruptures in the southern Santa Cruz Mountains, California: Journal of Geophysical Research, v. 102, p. 635–648.

Ramzan, S., and Yule, J.D., 2011, Paleoseismic investigation of the San Gorgonio Pass fault zone near Cabezon, California: Southern California Earthquake Center Annual Meeting Proceedings and Abstracts, v. 21.

Rubin, C.M., Lindvall, S.C., and Rockwell, T.K., 1998, Evidence for large earthquakes in metropolitan Los Angeles: Science, v. 281, p. 398–402.

Rymer, M.J., Tinsley, J.C., III, Treiman, J.A., Arrowsmith, J.R., Clahan, K.B., Rosinski, A.M., Bryant, W.A., Snyder, H.A., Fuis, G.S., Toké, N.A., and Bawden, G.W., 2006, Surface fault slip associated with the 2004 Parkfield, California, earthquake: Seismological Society of America Bulletin, v. 96, p. 11–27.

Salisbury, J. B., Arrowsmith, J R., Rockwell, T. K., Haddad, D., Zielke, O., & Madden, C. 2012a. The Climatic Role in Formation of Fault-Offset Geomorphic Features: Reliable Measurements for Slip-Per-Event Studies, European Geocsicences General Assembly, Vienna, Austria.

Salisbury, J.B., Rockwell, T.K., Middleton, T.J., and Hudnut, K.W., 2012b, LiDAR and field observations of slip distribution for the most recent surface ruptures along the central San Jacinto fault: Seismological Society of America Bulletin, v. 102, no. 2, p. 598–619.

Salyards, S.L., Sieh, K.E., and Kirschvink, J.L., 1992, Paleomagnetic measurement of non-brittle coseismic deformation across the San Andreas fault at Pallett Creek, California: Journal of Geophysical Research, v. 96, p. 12457–12470.

Scholz, C., 2002, The mechanics of earthquakes and faulting: Cambridge University Press, 496 p.

Seitz, G., 1999, The paleoseismology of the southern San Andreas fault at Pitman Canyon—implications for fault behavior and paleoseimic methodology: Eugene, University of Oregon, Ph.D. dissertation, 278 p.

Seitz, G.G., and Kent, G., 2004, Closing the gap between on and offshore paleoseismic records in the Lake Tahoe basin: U.S. Geological Survey, National Earthquake Hazards Reduction Program, Final Technical Report, 14 p.

Sharp, R.V., Lienkaemper, J.J., Bonilla, M.G., Burke, D.B., Fox, B.F., Herd, D.G., Miller, D.M., Morton, D.M., Ponti, D.J., Rymer, M.J., Tinsley, J.C., Yount, J.C., Kahle, J.E., Hart, E.W., and Sieh, K.E., 1982, Surface faulting in the central Imperial Valley in the Imperial Valley,

California, earthquake of October 15, 1979: U.S. Geological Survey Professional Paper 1254, p. 119–154, plate 1.

Sharp, R.V., Budding, K.E., Boatwright, J., Ader, M.J., Bonilla, M.G., Clark, M.M., Fumal, T.E., Harms, K.K., Lienkaemper, J.J., Morton, D.M., O'Neill, B.J., Ostergren, C.L., Ponti, D.J., Rymer, M.J., Saxton, J.L., and Sims, J.D., 1989, Surface faulting along the Superstition Hills fault zone and nearby faults associated with the earthquakes of November 24, 1987: Seismological Society of America Bulletin, v. 79, p. 252–281.

Sieh, K.E., 1978, Slip along the San Andreas fault associated with the great 1857 earthquake: Seismological Society of America Bulletin, v. 68, p. 1421–1448.

Sieh, K.E., Jones, L., Hauksson, E., Hudnut, K., Eberhart-Phillips, D., Heaton, T., Hough, S., Hutton, K., Kanamori, H., Lilje, A., Lindvall, S., McGill, S.F., Mori, J., Rubin, C., Spotila, J.A., Stock, J., Thio, H.K., Treiman, J., Wernicke, B., and Zachariasen, Z., 1993, Near-field investigations of the Landers earthquake sequence, April to July 1992: Science, v. 260, p. 171–176.

Simpson, G.D., Thompson, S.C., Noller, S., and Lettis, W.R., 1997, The northern San Gregorio fault zone—evidence for timing of late Holocene earthquakes near Seal Cove, California: Seismological Society of America Bulletin, v. 87, no. 5, p. 1158–1170.

Spotila, J.A., and Anderson, K.B., 2004, Fault interaction at the junction of the Transverse Ranges and eastern California shear zone—a case study of intersecting faults: Tectonophysics, v. 379, p. 43–60.

Treiman, J.A., 2002, Chino fault, Riverside and San Bernardino counties, California: California Geological Survey Fault Evaluation Report 247, 18 p., 3 pl.

Treiman, J.A., Kendrick, K.J., Bryant, W.A., Rockwell, T.K., and McGill, S.F., 2002, Primary surface rupture associated with the Mw 7.1 16 October 1999 Hector Mine earthquake, San Bernardino County, California: Seismological Society of America Bulletin, v. 92, p. 1171–1191.

Tucker, A.Z., and Dolan, J.F., 2001, Paleoseismologic evidence for a >8 ka age for the most recent surface rupture on the eastern Sierra Madre fault, northern Los Angeles metropolitan region: Seismological Society of America Bulletin, v. 91, p. 232–249.

Vadurro, G., Bickner, F., Lindberg, D., Manhart, G., Watt, C., 2006, Fault rupture and fold hazard evaluation of the Little Salmon fault and the College of the Redwoods Eureka Campus, southern Cascadia Subduction Zone fold and thrust belt, NW California: Friends of the Pleistocene, Pacific Cell 2006, p. 121-135.

Vaughan, P.R., Thorup, K.M., and Rockwell, T.K., 1999, Paleoseismology of theElsinore fault at Agua Tibia mountain, southern California: Seismological Society of America Bulletin, v. 89, no. 6, p. 1447–1457.

Walls, C., and Gath, E.M., 2001, Tectonic geomorphology and Holocene surface rupture on the Chino fault: Southern California Earthquake Center Annual Meeting, Proceedings and Abstracts, v. 21, p. 118.

Wallace, R.E., 1968, Notes on stream channels offset by the San Andreas fault, southern Coast Ranges, California, in Dickinson, W.R., and Grantz, A., eds., Proceedings of conference on geologic problems of the San Andreas fault system: Stanford University Publications in the Geological Sciences, v. 11, p. 6–21.

Weldon, R., and Scharer, K., 2009, Slip rates for the San Andreas fault between the Big Bend and the San Bernardino Valley, southern California: U.S. Geological Survey, National Earthquake Hazards Reduction Program, Final Technical Report, 10 p.

Weldon, R.J., II, Fumal, T.E., Powers, T., Pezzopane, S.K., Scharer, K.M., and Hamilton, J.C., 2002, Structure and earthquake offsets on the San Andreas fault at the Wrightwood, California paleoseismic site: Seismological Society of America Bulletin, Special Issue on Paleoseismology of the San Andreas Fault System, v. 92, p. 2704–2725.

Wells, D.L., and Coppersmith, K.J., 1994, New empirical relationships among magnitude, rupture length, rupture width, rupture area, and surface displacement: Seismological Society of America Bulletin, v. 84, p. 974–1002.

Wesnousky, S.G., 2008, Displacement and geometrical characteristics of earthquake surface ruptures: Seismological Society of America Bulletin, v. 98, p. 1609–1632.

Yule, J.D., and McBurnett, P.L., 2011, Paleoseismology and slip rate of the San Gorgonio Pass fault zone at Millard Canyon—Testing the likelihood of through-going San Andreas ruptures: Southern California Earthquake Center Annual Meeting Proceedings and Abstracts, v. 21.

Zachariasen, J. Z., and Prentice, C. S., 2008, Detailed mapping of the northern San Andreas fault using LiDAR imagery: U.S. Geological Survey, National Earthquake Hazards Reduction Program, Final Technical Report, 47 p.

Zhang, H., 2006, Paleoseismic studies of the northern San Andreas fault at Vedanta Marsh site, Olema, California: Kansas City, University of Missouri, Ph.D. dissertation.

Zhang, H., Niemi, T.M., and Fumal, T., 2006, A 3000-year record of earthquakes on the northern San Andreas fault at the Vedanta marsh site, Olema, California [abs.]: Seismological Research Letters, v. 77, no. 2, p. 248.

Zhang, P., Ellis, M., Slemmons, D.B., and Mao, F., 1990, Right-lateral displacements and the Holocene slip rate associated with prehistoric earthquakes along the southern Panamint Valley Fault Zone—implications for southern Basin and Range tectonics and coastal California deformation: Journal of Geophysical Research, v. 95, p. 4857–4872.

Zielke, O., and Arrowsmith, J.R., 2012, LaDiCaoz and LiDARimager -MATLAB GUIs for LiDAR data handling and lateral displacement measurement: Geosphere v.8, no. 1, p. 206-221, doi: 10.1130/GES00686.1.

Zielke, O., Arrowsmith, J.R., Grant-Ludwig, L.B., and Akciz, S.O., 2010, Slip in the 1857 and earlier large earthquakes along the Carrizo Segment, San Andreas fault: Science, v. 327, p. 1119–1121.

Zielke, O., Arrowsmith, J.R., Grant-Ludwig, L.B., and Akciz, S.O., 2012, High-resolution topography-derived offsets along the 1857 Fort Tejon earthquake rupture trace, San Andreas fault: Seismological Society of America Bulletin, v. 102, p. 1135–1154.

Tables

R1. Number and type of offset measurements compiled for each fault section.
R2. Number and type of offset measurements for recent historical ruptures.
R3. Displacement for the last event for UCERF 3 fault subsections: recent historical ruptures.
R4. "Best" estimate of displacement in the last event for UCERF 3 fault subsections: recent historical ruptures.
R5. Displacement for the last event for UCERF 3 fault subsections: older historical and prehistoric ruptures.
R6 "Best" estimate of displacement for the last event for UCERF 3 fault subsections: older historical and prehistoric ruptures.
R7. Repeated slip for a subsection from cumulative offset probability density functions of offset features.
R8. Repeated slip at a point from paleoseismology.
R9. Average displacement for large prehistoric or early historic surface rupturing earthquakes from geomorphology.

Table R1. Number and type of offset measurements compiled for each fault section.

[2011 CFM/ 2011, 2011 rev, and rev, faults that have been updated for the UCERF 3 fault model (*http://www.wgcep.org/components-fault_model*), subsection vertices that we have used were delivered by Kevin Milner to Arrowsmith in February 2012; CFM*, fault update based on the community fault model; alt 1 and 2, fault alternative that best fits location of offset data; MRE, most recent earthquake; USGS, U.S. Geological Survey; CDMG, California Division of Mines and Geology; CGS, California Geological Survey; Location maps and tables of offset versus distance can be found by clicking the links on the right side of the table, or in supplemental file R1-2; maps and graphs of offsets for UCERF 3 fault subsections can be found in supplemental file R6; [+]Upper plot is map of UCERF3 fault sections and selection buffer--in cyan. Lower plot is projected along strike distance versus offset. Circles at base indicate fault trace vertices]

Fault segment name	Number and type of offset measurements	Principal references	Location map	Offset versus distance[+]
Blackwater	**1 field**; MRE	M. Oskin, 2011, written commun.	Blackwater Map	Blackwater Offsets
Burnt Mountain	**7 field**; 1992 Landers rupture	Sieh and others, 1993; USGS, unpublished; CDMG, unpublished; Peterson and others, 2011; CGS, unpublished	Burnt Mountain Map	Burnt Mountain Offsets
Calico-Hidalgo (Calico)	**37 total offset measurements**: 27 field and 10 calculated; MRE and multiple event	Ganev and others, 2010	Calico Map	Calico (horiz.)
Camp Rock 2011	**95 field**; MRE (1992 Landers Earthquake)	Sieh and others, 1993; Caltech unpublished; Peterson and others, 2011	Camp Rock Map	Camp Rock Offsets
Chino alt 2	**2 paleoseismology**; MRE and multiple event	Walls and Gath, 2001; E. Gath, and C. Walls, 2011, written commun.; Treiman, 2001	Chino Map	Chino Offsets

Fault segment name	Number and type of offset measurements	Principal references	Location map	Offset versus distance+
Compton	**6 paleoseismology**; slip for each of last six events	Leon and others, 2009; Madden and others, this study	Compton Map	Compton Offsets Measurements are 19 km from the UCERF3 fault segment surface traces.
Elmore Ranch (includes Lone Tree and Kane Creek faults)	**126 field**; MRE (1987 Elmore Ranch Earthquake)	Sharp and others, 1989; Peterson and others, 2011; CGS, unpublished	Elmore Ranch Map	Elmore Ranch Offsets
Elsinore (Temecula) rev	**23 LiDAR**; MRE and multiple event	Haddad and others, 2011; Madden and others, this study	Elsinore Temecula Map	Elsinore Temecula Offsets
Elsinore (Julian)	**34 LiDAR**; LiDAR-derived; MRE and multiple	Haddad and others, 2011; Madden and others, this study	Elsinore Julian Map	Elsinore Julian Offsets
Emerson-Copper Mountain 2011 (Emerson)	**407 field**; MRE (1992 Landers Earthquake)	Sieh and others, 1993; CDMG, unpublished; Caltech, unpublished; USGS, unpublished; Peterson and others, 2011	Emerson Map	Emerson Offsets
Eureka Peak	**20 field**; MRE (1992 Landers Earthquake)	Sieh and others, 1993; Caltech, unpublished; USGS, unpublished; CDMG, unpublished; Peterson and others, 2011; CGS, unpublished	Eureka Peak Map	Eureka Peak Offsets
Garlock (West)	**184 LiDAR**; MRE (3-5 m) and multiple event (<40 m)	Haddad and others, 2011; Madden and others, this study	Garlock West Map	Garlock West Offsets
Garlock (Central)	**192 total offset measurements**; 124 field and 68 LiDAR; MRE and multiple event	Haddad and others, 2011; Madden and others, this study; McGill and Sieh, 1991; Haddad and others 2011; Madden and others, this study	Garlock Central Map	Garlock Central Offsets

Fault segment name	Number and type of offset measurements	Principal references	Location map	Offset versus distance+
Garlock (East)	**162 total offset measurements**: 101 field and 61 LiDAR; MRE and multiple event	Haddad and others, 2011; McGill and Sieh, 1991; Madden and others, this study	Garlock East Map	Garlock East Offsets
Green Valley 2011 CFM*	**1 paleoseismology**; MRE	Baldwin and Lienkaemper, 1999; Madden and others, this study	Green Valley Map	Green Valley Offset
Hayward (North) 2011 CFM*	**1 field**; multiple event and creep	J.J. Lienkaemper, 2012, written commun.	Hayward North Map	Hayward North Offsets
Hector Mine aka Lavic Lake	**154 field**; MRE (1999 Hector Mine Earthquake)	Treiman and others, 2002; CGS, unpublished	Hector Mine Map	Hector Mine Offsets
Homestead Valley 2011	**373 field**; MRE (1992 Landers Earthquake)	Sieh and others, 1993; Caltech, unpublished; USGS, unpublished; CDMG, unpublished; William Lettis Associates; unpublished; Peterson and others, 2011; CGS, unpublished	Homestead Valley Map	Homestead Valley Offsets
Hunter Mountain--Saline Valley (Hunter Mountain)	**1 field**; MRE	Oswald and Wesnousky, 2002; Madden and others, this study	Hunter Mountain-Map	Hunter Mountain-Offsets
Imperial	**122 field**; MRE (1979 Imperial Valley Earthquake)	Sharp and others, 1982; Peterson and others, 2011; CGS, unpublished	Imperial Map	Imperial Offsets
Incline Village 2011 CFM*	**1 paleoseismology;** MRE	Seitz and Kent, 2004; Madden and others, this study	Incline Village Map	Incline Village Offset

Fault segment name	Number and type of offset measurements	Principal references	Location map	Offset versus distance+
Johnson Valley (South) 2011 rev	**183 field**; MRE (1992 Landers Earthquake)	Sieh and others, 1993; Caltech, unpublished; USGS, unpublished; CDMG, unpublished; William Lettis Associates, unpublished; Peterson and others, 2011	Johnson Valley South Map	Johnson Valley South Offsets
Landers 2011 rev	**50 field**; MRE (1992 Landers Earthquake)	Sieh and others, 1993; Caltech, unpublished; USGS, unpublished; CDMG, unpublished; William Lettis Associates, unpublished; Peterson and others, 2011; CGS, unpublished	Landers Map	Landers Offsets
Lenwood-Lockhart-Old Woman Springs (Lenwood)	**12 field**; MRE and multiple event	Strane, M., unpublished	Lenwood Map	Lenwood Offsets
Little Salmon (Onshore)	**5 paleoseismology**; MRE and multiple event	Vadurro and others, 2006; Carver and Burke, 1988; Hemphill-Haley and Witter, 2004; Madden and others, this study	Little Salmon Onshore Map	Little Salmon Onshore Offsets
North Frontal (West)	**1 paleoseismology**; MRE	Spotilla and Anderson, 2004; Madden and others, this study	North Frontal West Map	North Frontal West Offset
Owens Valley	**145 LiDAR**; MRE and multiple event	Haddad and others, 2011; Madden and others, this study	Owens Valley Map	Owens Valley Offsets
Panamint Valley	**10 field**; MRE and multiple event	Zhang and others, 1990; Madden and others, this study	Panamint Valley Map	Panamint Valley Offsets
Pisgah-Bullion Mountain-Mesquite Lake (Bullion)	**78 field**; MRE (1999 Hector Mine Earthquake)	Treiman and others, 2002; CGS, unpublished	Bullion Mountain-Map	Bullion Mountain Offsets

Fault segment name	Number and type of offset measurements	Principal references	Location map	Offset versus distance+
Pisgah-Bullion Mountain-Mesquite Lake (Mesquite Lake)	**39 field**; MRE (1999 Hector Mine Earthquake)	Treiman and others, 2002; CGS, unpublished	Mesquite Lake Map	Mesquite Lake Offsets
Puente Hills	**6 paleoseismology**; MRE and slip for each of the two prior events	Leon and others, 2007; Madden and others, this study	Puente Hills Map	Puente Hills Offsets
Rodgers Creek-Healdsburg 2011 CFM*	**5 total offset measurements**: 3 field and 2 paleoseismology; MRE and multiple event	Hart and others, 1988, unpublished; Budding and others, 1991; Hecker and others, 2005; Schwartz D., 2012, oral commun.; Madden and others, this study	Rodgers Creek Map	Rodgers Creek Offsets
San Andreas (North Coast) 2011 CFM*	**14 total offset measurements**: 3 field, 5 paleoseismology; 5 LiDAR, 3 field,and 1 geophysiscs; MRE (1906 Earthquake), penultimate event and multiple event	Lawson, 1908; Baldwin, 1996; Baldwin and others, 2000; Green and others, 2003; Kelson and others, 2006; Zachariasen and others, 2008; Zhang and others, 2006; Madden and others, this study	San Andreas North Coast Map	San Andreas North Coast Offsets
San Andreas (Peninsula) 2011 CFM*	**3 paleoseismology** MRE, penultimate event, and multiple event	Hall and others, 1999; Madden and others, this study	San Andreas Peninsula Map	San Andreas Peninsula Offsets
San Andreas (Santa Cruz Mountains)	**4 total offsets**; 2 field and 2 paleoseismology; MRE (1906 Earthquake), penultimate event, and multiple event	Lawson, 1908; Prentice and Ponti, 1997; Fumal and others, 1999; Madden and others, this study	San Andreas Santa Cruz Mtns. Map	*See Supplemental File R6*
San Andreas (Creeping section) 2011 CFM*	**47 LiDAR**; Creeping	Salisbury and others, 2012a; Madden and others, this study	San Andreas Creeping Map	San Andreas Creeping Offsets

Fault segment name	Number and type of offset measurements	Principal references	Location map	Offset versus distance+
San Andreas (Parkfield)	**63 field offsets**; MRE (2004 Parkfield Earthquake)	Rymer and others, 2006; J.A. Treiman, unpublished; J.C. Tinsley, unpublished	San Andreas Parkfield Map	San Andreas Parkfield Offsets
San Andreas (Cholame) rev	**106 total offset measurements**; 15 field, 32 aerial photo, and 59 LiDAR; MRE and multiple event	Sieh, 1978; Lienkaemper, 2001; Zielke and others, 2010; Zielke and others, 2012.	San Andreas Cholame Map	San Andreas Cholame Offsets[1]
San Andreas (Carrizo) rev	**189 total offset measurements:**; 48 field, 134 LiDAR, and 7 LiDAR; MRE (1857 earthquake) and multiple event	Sieh, 1978; Lienkaemper, 2001; Zielke and others, 2010; Zielke and others, 2012; Liu and others, 2004; Liu-Zeng and others, 2006.	San Andreas Carrizo Map	San Andreas Carrizo Offsets[1]
San Andreas (Big Bend)	**51 total offset measurements**: 12 field and 39 LiDAR; MRE (1857 earthquake) and multi-event	Sieh, 1978; Zielke and others, 2012	San Andreas Big Bend Map	San Andreas Big Bend Offsets
San Andreas (Mojave north)	**21 total offset measurements:** 19 LiDAR and 2 field; MRE (1857 Earthquake) and multiple event	Sieh, 1978; Zielke and others, 2012	San Andreas Mojave Map	San Andreas Mojave Offsets
San Andreas (Mojave south)	**124 total offset measurements**; 95 LiDAR,19 field and 10 paleoseismology; MRE, penultimate, and multi-event	Salyards and others, 1992; Seitz, 1999; Sieh, 1978; Weldon and others, 2002; Weldon and Scharer, 2009; Zielke and others, 2012	San Andreas Mojave South Map	San Andreas Mojave South Map
San Andreas (Coachella) rev	**88 total offset measurements**: 72 Field and 16 LiDAR; MRE and multi-event	Williams, P., and others, unpublished	San Andreas Coachella Map	San Andreas Coachella Offsets
San Cayetano	**1 paleoseismology**; MRE	Dolan and Rockwell, 2001; Madden and others, this study	San Cayetano Map	San Cayetano Offsets
San Gorgonio Pass	**2 paleoseismology**; MRE and multiple events	Ramzan and Yule, 2011; Yule and McBurnett, 2011	San Gorgonio Pass Map	San Gorgonio Pass Offsets

Fault segment name	Number and type of offset measurements	Principal references	Location map	Offset versus distance+
San Gregorio (North) 2011 CFM*	**2 paleoseismology**; MRE and penultimate	Simpson and others, 1997; Madden and others, this study	San Gregorio North Map	San Gregorio North Offsets
San Jacinto (Clark rev)	**494 total offset measurements**; 229 field, 219 LiDAR, and 45 aerial photo; MRE and multiple events	Salisbury and others, 2012b	San Jacinto Clark Map	San Jacinto Clark Offsets
San Jacinto (Borrego)	**140 field**; MRE (1968 Borrego Mountain Earthquake)	Clark, 1972; Peterson and others, 2011	San Jacinto Borrego Map	San Jacinto Borrego Offsets
Sierra Madre (San Fernando)	**145 field**; MRE (1971 Sylmar Earthquake)	Barrows and others, 1973; Madden and others, this study	Sierra Madre San Fernando Map	Sierra Madre San Fernando Offsets
Sierra Madre	**4 paleoseismology**; MRE, penultimate, and multiple events	Rubin and others, 1998; Tucker and Dolan, 2001; J.F. Dolan, unpublished; Madden and others, this study	Sierra Madre Map	Sierra Madre Offsets
Simi-Santa Rosa	**2 paleoseismology;** MRE and multiple events	Gonzalez and Rockwell, 1991; Madden and others, this study	Simi-Santa Rosa Map	Simi-Santa Rosa Offsets
Superstition Hills	**270 field**; MRE (1987 Superstition Hills Earthquake)	Sharp and others, 1989; Peterson and others, 2011	Superstition Hills Map	Superstition Hills Offsets
Whittier alt 1	**1 paleoseismology;** MRE	E.M. Gath, 2011, written commun.; Gath and others, 1992; Patterson and Rockwell, 1993; Dolan and others, 2007	Whittier Map	Whittier Offsets

[1]Assumed symmetric uncertainty for Zielke and others, 2012.

Table R2. Number and type of offset measurements for recent historical ruptures.
[EQ, earthquake; LE, Landers Earthquake; HE, Hector Mine Earthquake]

Earthquake	Fault segment names	Number and type of offsets	Principal references	Location map	Offset versus distance+
1968 Borrego Mountain earthquake	Coyote Creek (Borrego Mtn section of San Jacinto Fault)	140 offsets; field-derived	Clark, 1972 Peterson and others, 2011	Borrego Mtn. EQ Map	Borrego Mtn. EQ Offsets
1971 Sylmar earthquake	Sierra Madre (San Fernando)	148 offsets; field-derived	Barrows and others, 1973; Madden and others, this study	Sylmar EQ Map	Sylmar EQ Offsets
1979 Imperial Valley earthquake	Imperial Valley	122 offsets; field derived	Sharp and others, 1982; Peterson and others,, 2011	Imperial Valley EQ Map	Imperial Valley EQ Offsets
1987 Elmore Ranch-Superstition Hills earthquake	--Superstition Hills Fault --Elmore Ranch Fault	269 offsets; field-derived	Sharp and others, 1989; Peterson and others, 2011	Elmore Ranch-Superstition Hills EQ Map	Elmore Ranch-Superstition Hills EQ Offsets
1992 Landers earthquake`	--Camp Rock --Emerson --Homestead Valley --Johnson Valley --Burnt Mountain --Eureka Peak	1135 offsets; field-derived	See individual fault references above	Landers EQ Map	LE Camp Rock LE Emerson LE Homestead Valley LE Johnson Valley LE Eureka Peak Burnt Mountain Offsets
1999 Hector Mine earthquake	--Lavic Lake (called Hector Mine in UCERF3 v.3.1 fault database) --Mesquite Lake --Pisgah --Bullion	279 offsets; field-derived	See individual fault references above	Hector Mine EQ Map	HE Lavic Lake HE Mesquite Lake HE Pisgah HE Bullion Offsets
2004 Parkfield earthquake	San Andreas	62 offsets; field-derived	Rymer and others, 2006; J.A. Treiman, unpublished; J.C. Tinsley, unpublished	Parkfield EQ Map	Parkfield EQ Offsets

Table R3. Displacement for the last event for UCERF 3 fault subsections: recent historical ruptures.

["Recent historical ruptures" are all ruptures that were followed by a dedicated post-seismic response to map offsets; COPD, cumulative offset probability density; yellow shading, recommended value; green shading, agreement of maximum slip and highest COPD peak constructed by at least two offset measurements; orange shading, maximum slip and max COPD differ by more than the uncertainty of the mean, but less than a about a factor of two; uncertainty for mean single-event offsets represents standard deviation of uncertainties for S measurements in a subsection; uncertainty for maximum slip represents measurement uncertainty; 0.001 m uncertainty applied to maximum slip if no uncertainty measurement had been included in the source data; figures showing results for each subsection in supplemental files R6]

Fault name (section name)	Last rupture (A.D.)	Subsection	Number of single-event offset measurements	Mean single-event offset (m)	Standard deviation ± (m)	Maximum slip (m)	Uncertainty ± (m)	All offset COPD maximum (m)	Highest distinctive COPD (number of measurements) (m)	Best estimate (m)	Uncertainty (m)	Comments
Burnt Mtn	1992	0	7	0.04	0.004	0.06	0.001	0.04	0.06 (2)	0.06	0.001	
Camp Rock-2011	1992	0	1	0.71	0.08	0.71	0.08	0.7	Single measurement	0.71	0.08	Minimum
Camp-Rock-2011	1992	1	45	0.45	0.07	1.17	0.07	0.3	1.05 (5)	1.17	0.07	
Camp-Rock-2011	1992	2	22	0.29	0.05	0.69	0.07	0.35	0.66 (3)	0.69	0.07	
Elmore-Ranch	1987	4	23	0.043	0.001	0.121	0.001	0.014	No distinctive peaks.	0.121	0.001	
Elmore-Ranch	1987	5	17	0.028	0.001	0.057	0.001	0.02	0.34 (2)	0.057	0.001	
Emerson-Copper-Mtn-2011	1992	6	1	0.20	0.01	0.2	0.01	0.20	Single measurement.	0.2	0.01	Minimum
Emerson-Copper-Mtn-2011	1992	7	37	1.01	0.21	3.9	0.02	1.1	COPD maximum and highest COPD are the same.	3.9	0.02	
Emerson-Copper-Mtn-2011	1992	8	165	1.02	0.29	5.30	0.001	0.15	4.1 (7)	5.30	0.001	

Fault name (section name)	Last rupture (A.D.)	Subsection	Number of single-event offset measurements	Mean single-event offset (m)	Standard deviation ± (m)	Maximum slip (m)	Uncertainty ± (m)	All offset COPD maximum (m)	Highest distinctive COPD (number of measurements) (m)	Best estimate (m)	Uncertainty (m)	Comments
Emerson-Copper-Mtn-2011	1992	9	39	1.32	0.43	3.72	0.3	0.09	3.1 (6)	3.72	0.3	
Emerson-Copper-Mtn-2011	1992	10	51	0.5	0.11	3.2	0.3	0.03	3.0 (2)	3.20	0.30	
Eureka-Peak	1992	1	8	0.07	0.02	0.19	0.01	0.01	No distinctive peaks	0.19	0.01	
Eureka-Peak	1992	2	12	0.11	0.01	0.21	0.02	0.03	0.205 (2)	0.21	0.03	
Hector-Mine	1999	0	27	0.63	0.07	2.6	0.1	0.4	No distinctive peaks	2.6	0.1	
Hector-Mine	1999	1	9	1.77	0.38	2.50	0.30	2.30	COPD maximum and highest COPD are the same.	2.50	0.30	
Homestead-Valley-2011	1992	2	7	0.56	0.10	1.04	0.25	0.28	No distinctive peaks.	1.04	0.25	
Homestead-Valley-2011	1992	3	165	0.37	0.11	2.92	0.15	0.25	1.8 (3)	2.92	0.15	
Homestead-Valley-2011	1992	4	22	1.99	0.26	3.45	0.2	3.1	3.1 (6)	3.45	0.2	Minimum . Multiple strands; buffer not wide

Fault name (section name)	Last rupture (A.D.)	Subsection	Number of single-event offset measurements	Mean single-event offset (m)	Standard deviation ± (m)	Maximum slip (m)	Uncertainty ± (m)	All offset COPD maximum (m)	Highest distinctive COPD (number of measurements) (m)	Best estimate (m)	Uncertainty (m)	Comments
												enough to capture strand to NE.
Homestead-Valley-2011	1992	5	84	0.41	0.09	2.85	0.22	0.30	2.7 (2)	2.85	0.22	Minimum. Multiple strands; buffer not wide enough to capture strand to NE.
Imperial	1979	4	2	0.295	0.01	0.55	0.01	0.04	No distinctive peaks.	0.55	0.01	Minimum
Imperial	1979	5	11	0.657	0.010	0.782	0.01	0.512	0.759 (2)	0.782	0.01	
Imperial	1979	6	13	0.542	0.01	0.732	0.01	0.60	0.6 (2)	0.732	0.01	
Imperial	1979	7	18	0.237	0.010	0.525	0.01	0.22	No distinctive peaks.	0.525	0.01	
Imperial	1979	8	16	0.119	0.01	0.23	0.01	0.022	No distinctive peaks.	0.2	0.01	

Fault name (section name)	Last rupture (A.D.)	Subsection	Number of single-event offset measurements	Mean single-event offset (m)	Standard deviation ± (m)	Maximum slip (m)	Uncertainty ± (m)	All offset COPD maximum (m)	Highest distinctive COPD (number of measurements) (m)	Best estimate (m)	Uncertainty (m)	Comments
Johnson-Valley-(So)-2011-rev	1992	0	28	0.76	0.06	2.30	0.1	0.05	2.25 (3)	2.30	0.1	
Johnson-Valley-(So)-2011-rev	1992	1	58	1.09	0.10	2.92	0.10	2.88	COPD maximum and highest COPD are the same.	2.92	0.1	
Johnson-Valley-(So)-2011-rev	1992	2	38	0.69	0.08	3.00	0.30	0.01	3.0 (2)	3.0	0.3	
Landers-2011-rev	1992	0	19	0.73	0.11	2.15	0.10	0.20	No distinctive peaks.	2.15	0.1	
Landers-2011-rev	1992	1	22	1.06	0.16	2.90	0.01	0.90	2.1 (2)	2.90	0.01	
Pisgah-Bullion-Mtn-Mesquite-Lk	1999	4	5	0.11	0.02	0.17	0.03	0.12	0.12 (2)	0.17	0.03	
Pisgah-Bullion-Mtn-Mesquite-Lk	1999	5	20	0.18	0.03	0.70	0.05	0.02	No distinctive peaks.	0.7	0.05	
Pisgah-Bullion-Mtn-Mesquite-Lk	1999	6	57	0.76	0.13	2.45	0.4	1.00	1.85 (5)	2.45	0.4	
San-Andreas-(Parkfield)	2004.	0	1	0.008	0.001	0.008	0.01	0.008	Single measurement	0.008	0.001	Minimum
San-Andreas-(Parkfield)	2004	1	7	0.011	0.002	0.018	0.003	0.01	0.0175 (2)	0.0175	0.003	

Fault name (section name)	Last rupture (A.D.)	Subsection	Number of single-event offset measurements	Mean single-event offset (m)	Standard deviation ± (m)	Maximum slip (m)	Uncertainty ± (m)	All offset COPD maximum (m)	Highest distinctive COPD (number of measurements) (m)	Best estimate (m)	Uncertainty (m)	Comments
San-Andreas-(Parkfield)	2004	2	8	0.031	0.001	0.043	0.001	0.03	0.043 (2)	0.043	0.001	
San-Andreas-(Parkfield)	2004	3	20	0.012	0.001	0.026	0.001	0.004	0.0215 (3)	0.026	0.001	
San-Andreas-(Parkfield)	2004.	4	21	0.019	0.001	0.03	0.001	0.02	0.030 (4)	0.03	0.001	
San-Andreas-(Parkfield)	2004	6	2	0.063	0.001	0.07	0.001	0.055	No distinctive peaks	0.07	0.001	
San-Jacinto-(Borrego)	1968	0	17	0.068	0.001	0.36	0.001	0.03	No distinctive peaks	0.36	0.001	
San-Jacinto-(Borrego)	1968	1	16	0.107	0.001	0.29	0.001	0.032	0.2 (2)	0.29	0.001	
San-Jacinto-(Borrego)	1968	2	17	0.046	0.001	0.100	0.001	0.05	0.08 (3)	0.1	0.001	
San-Jacinto-(Borrego)	1968.	3	34	0.078	0.001	0.24	0.001	0.05	0.21 (2)	0.24	0.001	
San-Jacinto-(Borrego)	1968	4	14	0.015	0.001	0.05	0.001	0.02	0.04 (2)	0.05	0.001	
San-Jacinto-(Borrego)	1968	5	8	0.014	0.001	0.045	0.001	0.03	No distinctive peaks	0.045	0.001	
Sierra-Madre-(San-Fernando)	1971.	0	54	0.46	0.01	1.6	0.01	0.2	1.0 (2)	1.6	0.01	
Sierra-Madre-(San-Fernando)	1971	1	62	0.39	0.01	1.3	0.01	0.3	0.07 (4)	1.3	0.01	
Sierra-Madre-(San-Fernando)	1971	2	12	0.33	0.01	1.15	0.01	0.20	No distinctive peaks	1.15	0.01	

Fault name (section name)	Last rupture (A.D.)	Subsection	Number of single-event offset measurements	Mean single-event offset (m)	Standard deviation ± (m)	Maximum slip (m)	Uncertainty ± (m)	All offset COPD maximum (m)	Highest distinctive COPD (number of measurements) (m)	Best estimate (m)	Uncertainty (m)	Comments
Superstition-Hills	1987	0	23	0.05	0.001	0.216	0.001	0.02	0.08 (2)	0.22	0.001	
Superstition-Hills	1987	1	41	0.188	0.001	0.641	0.001	0.02	0.64 (2)	0.641	0.001	
Superstition-Hills	1987.	2	57	0.288	0.001	0.9	0.001	0.02	0.59 (5)	0.9	0.001	
Superstition-Hills	1987	3	57	0.354	0.001	0.895	0.001	0.04	0.6 (4) small peak; 0.5 (7+) large peak.	0.895	0.001	
Superstition-Hills	1987	4	36	0.1	0.001	0.424	0.001	0.04	0.25 (2)	0.424	0.001	
Superstition-Hills	1987	5	2	0.185	0.001	0.206	0.001	0.16	No distinctive peaks	0.206	0.001	

Table R4. "Best" estimate of displacement in the last event for UCERF 3 fault subsections: recent historical ruptures.

["Recent historical ruptures" are all ruptures that were followed by a dedicated post-seismic response to map offsets; *2011 CFM/ 2011, mapped fault based on Community Fault Model or updated UCERF 3 fault model (*http://www.wgcep.org/components-fault_model*, subsection vertices that we have used were delivered by Kevin Milner to Arrowsmith in February 2012; alt 1 and 2, fault alternative that best fit offset data;]

Fault name (section name) v3.2	Subsection	Best estimate of offset (m)	Uncertainty + (m)	Uncertainty - (m)	Last rupture (calendar year A.D.)
Burnt-Mtn	0	0.06	0.001	0.001	1992
Camp-Rock-2011	0	0.71	0.08	0.08	1992
Camp-Rock-2011	1	1.17	0.07	0.07	1992
Camp-Rock-2011	2	0.69	0.07	0.07	1992
Elmore-Ranch	4	0.121	0.001	0.001	1987
Elmore-Ranch	5	0.057	0.001	0.001	1987
Emerson-Copper-Mtn-2011	6	0.2	0.01	0.01	1992
Emerson-Copper-Mtn-2011	7	3.9	0.02	0.02	1992
Emerson-Copper-Mtn-2011	8	5.30	0.001	0.001	1992
Emerson-Copper-Mtn-2011	9	3.72	0.3	0.3	1992
Emerson-Copper-Mtn-2011	10	3.20	0.30	0.30	1992
Eureka-Peak	1	0.19	0.01	0.01	1992
Eureka-Peak	2	0.21	0.03	0.03	1982
Hector-Mine	0	2.6	0.1	0.1	1999
Hector-Mine	1	2.50	0.30	0.30	1999
Homestead-Valley-2011	2	1.04	0.25	0.25	1992
Homestead-Valley-2011	3	2.92	0.15	0.15	1992
Homestead-Valley-2011	4	3.45	0.2	0.2	1992
Homestead-Valley-2011	5	2.85	0.22	0.22	1992
Imperial	4	0.55	0.01	0.01	1979
Imperial	5	0.782	0.01	0.01	1979
Imperial	6	0.732	0.01	0.01	1979
Imperial	7	0.525	0.01	0.01	1979
Imperial	8	0.2	0.01	0.01	1979
Johnson-Valley-(So)-2011-rev	0	2.30	0.1	0.1	1992
Johnson-Valley-(So)-2011-rev	1	2.92	0.1	0.1	1992

Fault name (section name) v3.2	Subsection	Best estimate of offset (m)	Uncertainty + (m)	Uncertainty - (m)	Last rupture (calendar year A.D.)
Johnson-Valley-(So)-2011-rev	2	3.0	0.3	0.3	1992
Landers-2011-rev	0	2.15	0.1	0.1	1992
Landers-2011-rev	1	2.90	0.01	0.01	1992
Pisgah-Bullion-Mtn-Mesquite-Lk	4	0.17	0.03	0.03	1999
Pisgah-Bullion-Mtn-Mesquite-Lk	5	0.7	0.05	0.05	1999
Pisgah-Bullion-Mtn-Mesquite-Lk	6	2.45	0.4	0.4	1999
San-Andreas-(Parkfield)	0	0.008	0.001	0.001	2004
San-Andreas-(Parkfield)	1	0.0175	0.003	0.003	2004
San-Andreas-(Parkfield)	2	0.043	0.001	0.001	2004
San-Andreas-(Parkfield)	3	0.026	0.001	0.001	2004
San-Andreas-(Parkfield)	4	0.03	0.001	0.001	2004
San-Andreas-(Parkfield)	6	0.07	0.001	0.001	2004
San-Jacinto-(Borrego)	0	0.36	0.001	0.001	1968
San-Jacinto-(Borrego)	1	0.29	0.001	0.001	1968
San-Jacinto-(Borrego)	2	0.1	0.001	0.001	1968
San-Jacinto-(Borrego)	3	0.24	0.001	0.001	1968
San-Jacinto-(Borrego)	4	0.05	0.001	0.001	1968
San-Jacinto-(Borrego)	5	0.045	0.001	0.001	1968
Sierra-Madre-(San-Fernando)	0	1.6	0.01	0.01	1971
Sierra-Madre-(San-Fernando)	1	1.3	0.01	0.01	1971
Sierra-Madre-(San-Fernando)	2	1.15	0.01	0.01	1971
Superstition-Hills	0	0.22	0.001	0.001	1987
Superstition-Hills	1	0.641	0.001	0.001	1987
Superstition-Hills	2	0.9	0.001	0.001	1987
Superstition-Hills	3	0.895	0.001	0.001	1987
Superstition-Hills	4	0.424	0.001	0.001	1987
Superstition-Hills	5	0.206	0.001	0.001	1987

Table R5. Displacement for the last event for UCERF3 fault subsections: older historical and prehistoric ruptures.

["Older historical and prehistoric ruptures" are defined as all ruptures where offset measurements are based on geomorphology and paleoseismology; COPD, cumulative offset probability density; yellow shading, recommended value; green shading, mean for single-event offsets and COPD maximum are within uncertainty of mean; orange shading, mean for single event offsets and COPD differ by more than the uncertainty of the mean, but less than a factor of two; red shading, mean for single event offsets differ by more than a factor of two; no color, single measurement for subsections; uncertainty for mean single event offsets represents standard deviation of uncertainties for single-event offsets in a subsection; uncertainty for COPD based on uncertainty for mean single-event offsets; S, single event offset (hand-selected based on local minimum offset value); S-M, offset from single or multiple events cannot be clearly discerned; M, offset from multiple events; offsets for the creeping and Coachella sections of the San Andreas Fault are maximum values because they include slip in the last event plus creep since the last event; figures showing results for each subsection in supplemental files R6]

Fault name (section name)	Last rupture	Subsection	Number of single-event offset measurements	Mean single-event offset (m)	Standard deviation ± (m)	All offset COPD maximum (m)	Best estimate (m)	Uncertainty (m)	Comments
Blackwater	Unknown	8	1	2.0	0.1	2.0	2.0	0.1	Used single 'S' measurement
Calico-Hidalgo	0.6-2.0 ka	11	3	1.6	0.4	5.4	1.6	0.4	
Calico-Hidalgo	0.6-2.0 ka	12	9	1.9	0.4	1.6	1.9	0.4	Two low COPD peaks. Mean encompasses peaks and matches estimate of slip in last event from Ganev and others, 2010
Chino-alt-2	At least two earthquakes in 14.2 ka	1	1	2.5	0.4	2.5	2.5	0.4	Used single 'S' measurements
Compton	0.7-1.75 ka	2	6	2.8	0.9	2.4	2.4	+0.8/-0.6	Used slip in last event calculated by Leon and others (2009). Mean, COPD, and calculated slip all within uncertainty of mean
Elsinore-(Julian)	700-1700 yrs BP	5	1	2.0	0.3	4.9	2.0	0.3	Used single 'S' measurement
Elsinore-(Julian)	700-1700 yrs BP	7	8	1.6	0.3	1.6	1.6	0.3	
Elsinore-(Temecula)-rev	1655 A.D. - 1810 A.D.	4	13	1.3	0.3	1.8	1.8	0.5	Strong COPD peak includes some 'S-M' values. This suggests that mean is a minimum and that COPD better represents slip in last event. Uncertainty captures width of COPD peak.

Fault name (section name)	Last rupture	Subsection	Number of single-event offset measurements	Mean single-event offset (m)	Standard deviation ± (m)	All offset COPD maximum (m)	Best estimate (m)	Uncertainty (m)	Comments
Elsinore-(Temecula)-rev	1655 A.D. - 1810 A.D.	5	4	1.8	0.3	2.3	2.0	0.5	Maximum and secondary COPD form double peak. Secondary peak includes mean of 'S' values. Best guess is 2.0 m, which splits difference between mean and COPD. Uncertainty captures both COPD peaks.
Garlock-(Central)	1450 A.D. - 1640 A.D.	11	16	2.1	0.5	2.8	2.8	1.0	Wide distribution of 'S' and 'S-M' offsets. COPD higher than mean due to several high quality measurements at upper end of the range. Used COPD with large uncertainty to include mean and high quality offsets in best estimate.
Garlock-(Central)	1450 A.D. - 1640 A.D.	14	10	2.9	0.6	5.1	2.9	0.6	Wide distribution of 'S' measurements (smearing). Clusters of offsets around 3 m and 5 m. COPD max at 5 m, includes 'S-M' and 'M' measurements, and includes several high-quality measurements. Recommend using mean as best estimate; this is also more consistent with last slip on adjacent subsections. COPD value should also be used as an alternative.
Garlock-(Central)	1450 A.D. - 1640 A.D.	15	6	3.3	0.6	3.5	3.5	0.6	Good COPD peak. Slightly lower mean suggests that some S-M measurements are actually from the last event at the mean based on only S measurements is a minimum. COPD uncertainty based on mean uncertainty.

Fault name (section name)	Last rupture	Subsection	Number of single-event offset measurements	Mean single-event offset (m)	Standard deviation ± (m)	All offset COPD maximum (m)	Best estimate (m)	Uncertainty (m)	Comments
Garlock-(Central)	1450 A.D. - 1640 A.D.	16	1	2.5	1.3	15.3	2.5	1.3	Used single 'S' measurement. COPD based on two 'M' offsets.
Garlock-(Central)	1450 A.D. - 1640 A.D.	17	16	2.7	0.8	2.7	2.7	0.8	Good COPD peak.
Garlock-(Central)	1450 A.D. - 1640 A.D.	18	7	2.8	0.8	2.7	2.8	0.8	Broad scatter of 'S' measurements (smearing). Maximum COPD peak centered on single high-quality measurement.
Garlock-(East)	Post 1490 A.D.	4	5	2.3	0.7	3.6	3.6	0.5	OK COPD peak based on two high-quality offsets. Mean based on range of offsets between ~1 and ~4m from the same area. Lower values may represent localized variation in slip, decreasing mean.
Garlock-(East)	Post 1490 A.D.	5	44	2.5	0.7	3.2	3.2	1.0	Broad scatter of offsets between ~1 m and ~6 m. Strong maximum COPD peak. Overlapping 'S' and 'S-M' offsets suggest that mean is a minimum.
Garlock-(East)	Post 1490 A.D.	6	11	2.5	0.9	3.6	2.5	0.9	Two distinct low offset clusters. Mean centered on lower cluster and maximum COPD peak centered on higher cluster. We interpret lower cluster represents slip in last event.
Garlock-(East)	Post 1490 A.D.	7	3	2.2	0.6	2.9	2.9	0.5	Good COPD peak. Mean is minimum due to low outlier. COPD uncertainty based on width of peak.
Garlock-(West)	Post 1450 A.D.	2	1	3.5	1.5	10.2	3.5	1.5	Used single 'S' measurement. COPD based on multiple 'S-M' or 'M' offsets.
Garlock-(West)	Post 1450 A.D.	6	2	2.7	1.9	10.9	2.7	1.9	Maximum COPD peak based on a cluster of 'M' offsets.

Fault name (section name)	Last rupture	Subsection	Number of single-event offset measurements	Mean single-event offset (m)	Standard deviation ± (m)	All offset COPD maximum (m)	Best estimate (m)	Uncertainty (m)	Comments
Garlock-(West)	Post 1450 A.D.	7	1	2.8	0.8	7.2	2.8	0.8	Used single 'S' measurement. COPD based on mulyiple 'S-M' or 'M' offsets.
Garlock-(West)	Post 1450 A.D.	10	4	1.8	0.9	3.9	3.9	1.0	Strong maximum COPD peak. Mean forms shoulder on maximum COPD peak. COPD most likely represents slip in last event, but can't rule out that mean represents smaller event. COPD uncertainty based on width of curve.
Garlock-(West)	Post 1450 A.D.	11	12	1.9	0.8	7.2	1.9	0.8	Maximum COPD curve based on high quality 'M' offsets. Next highest subpeak is consistent with mean.
Garlock-(West)	Post 1450 A.D.	12	3	2.0	0.8	5.7	2.0	0.8	Mean is consistent with a strong COPD peak. Peak at 5.7 is based on cluster of 'M'" offsets.
Garlock-(West)	Post 1450 A.D.	13	1	2.6	0.7	5.1	2.6	0.7	Used single 'S' measurement. COPD based on multiple "S-M" or "M" offsets.
Green-Valley-2011-CFM	1573 A.D. - 1799 A.D.	5	1	1.4	0.2	1.4	1.4	0.2	Used single 'S' measurement.
Hunter-Mountain-Saline-Valley	Unknown	7	1	2.0	0.5	2.0	2.0	0.5	Used single 'S' measurement.
Incline-Village-2011-CFM	Post 1500 A.D.	2	1	2.8	0.5	2.8	2.8	0.5	Used single 'S' measurement.

Fault name (section name)	Last rupture	Subsection	Number of single-event offset measurements	Mean single-event offset (m)	Standard deviation ± (m)	All offset COPD maximum (m)	Best estimate (m)	Uncertainty (m)	Comments
Lenwood-Lockhart-Old-Woman-Springs	1.8 +/-0.2 ka	7	1	2.4	0.5	2.4	2.4	0.5	Used single 'S' measurement.
Lenwood-Lockhart-Old-Woman-Springs	1.8 +/-0.2 ka	8	1	3.5	0.5	3.5	3.5	0.5	Used single 'S' measurement.
Lenwood-Lockhart-Old-Woman-Springs	1.8 +/-0.2 ka	9	3	3.5	0.5	3.7	3.7	0.5	Nice maximum COPD peak
Little-Salmon-(Onshore)	Post 400-500 yr BP	1	4	2.6	0.5	3.8	4.4	0.8	Used slip in last event constrained by paleoseismic studies.
Little-Salmon-(Onshore)	Post 400-500 yr BP	2	1	5.6	0.5	5.6	5.6	0.5	Used single 'S' measurement.
North-Frontal--(West)	Post B.C. 9220	5	1	1.7	0.5	1.7	1.7	0.5	Used single 'S' measurement.
Owens-Valley	1872 A.D.	4	2	2.2	0.9	6.9	2.2	0.9	Mean represents lowest cluster of offsets and is consistent with a secondary COPD peak. Maximum COPD peak is based on a single high quality offset.
Owens-Valley	1872 A.D.	9	1	2.0	0.8	7.0	2.0	0.8	Used single 'S' measurement. COPD based on multiple "S-M" or "M" offsets.
Owens-Valley	1872 A.D.	14	3	2.3	1.1	2.2	2.3	1.1	

Fault name (section name)	Last rupture	Subsection	Number of single-event offset measurements	Mean single-event offset (m)	Standard deviation ± (m)	All offset COPD maximum (m)	Best estimate (m)	Uncertainty (m)	Comments
Owens-Valley	1872 A.D.	15	3	2.2	1.0	3.0	3.1	1.0	Good maximum COPD peak. Mean is a minimum due to low outliers.
Panamint-Valley	1400 A.D. - 1500 A.D.	5	2	3.3	0.5	3.3	3.3	0.5	
Panamint-Valley	1400 A.D. - 1500 A.D.	6	3	3.0	0.5	3.0	3.0	0.5	
Puente-Hills-(Santa-Fe-Springs)	0.2 - 0.3 ka	1	6	2.9	0.6	2.4	3.0	0.7	Averaged slip in last event from two paleoseimic sites (Leon and others, 2007).
Rodgers Creek-Healdsburg-2011-CFM	Post 1690 A.D. (Likely after 1750 A.D.)	2	1	2.0	0.3	2.0	2.0	0.3	Used single 'S' measurement.
Rodgers-Creek---Healdsburg-2011-CFM	Post 1690 A.D. (Likely after 1750 A.D.)	8	1	1.0	0.5	1.0	1.0	0.5	Used single 'S' measurement.
San-Andreas-(North-Coast)-2011-CFM	1906 A.D.	3	2	3.1	0.3	3.1	3.1	0.3	
San-Andreas-(North-Coast)-2011-CFM	1906 A.D.	15	1	3.6	0.5	3.6	3.6	0.5	Used single 'S' measurement.

Fault name (section name)	Last rupture	Subsection	Number of single-event offset measurements	Mean single-event offset (m)	Standard deviation ± (m)	All offset COPD maximum (m)	Best estimate (m)	Uncertainty (m)	Comments
San-Andreas-(North-Coast)-2011-CFM	1906 A.D.	16	4	3.2	0.5	3.6	3.2	0.5	
San-Andreas-(Peninsula)-2011-CFM	1906 A.D.	6	2	3.7	0.7	3.3	3.7	0.7	Poor COPD peaks due to limited number of measurements.
San-Andreas-(Creeping-Section)-2011-CFM	1906 A.D.?	1	1	3.2	0.4	4.2	3.2	0.4	Used single 'S' measurement. COPD based on multiple "S-M" or "M" offsets.
San-Andreas-(Creeping-Section)-2011-CFM	Unknown	3	1	3.9	0.3	3.9	3.9	0.3	Used single 'S' measurement.
San-Andreas-(Creeping-Section)-2011-CFM	Unknown	4	1	2.1	0.2	9.4	2.1	0.2	Used single 'S' measurement. COPD based on multiple "S-M" or "M" offsets.
San-Andreas-(Creeping-Section)-2011-CFM	Unknown	18	2	2.9	0.4	5.0	2.9	0.4	Maximum COPD based on only two measurements.
San-Andreas-(Cholame)-rev	1857 A.D.	6	2	3.7	0.7	3.3	3.7	0.7	

Fault name (section name)	Last rupture	Subsection	Number of single-event offset measurements	Mean single-event offset (m)	Standard deviation ± (m)	All offset COPD maximum (m)	Best estimate (m)	Uncertainty (m)	Comments
San-Andreas-(Cholame)-rev	1857 A.D.	7	4	3.5	0.6	4.5	4.5	1.0	Good COPD peak. Mean may be influenced by local minimum slip values and is therefore considered a minimum. COPD uncertainty based on width of curve.
San-Andreas-(Cholame)-rev	1857 A.D.	8	9	3.4	0.7	5.4	3.4	0.7	Mean is consistent with strong secondary COPD peak. Maximum COPD peak centered on cluster of larger offsets, and is amplified by a high quality measurement.
San-Andreas-(Cholame)-rev	1857 A.D.	9	2	3.9	0.9	6.2	3.9	0.9	Weak maximum COPD is peak is based on only two measurements.
San-Andreas-(Cholame)-rev	1857 A.D.	10	3	1.4	0.3	6.2	1.4	0.3	Maximum COPD is weak. Mean is consistent with second highest COPD peak.
San-Andreas-(Carrizo)-rev	1857 A.D.	0	1	5.0	0.8	9.2	5.0	0.8	Used single 'S' measurement. COPD based on multiple "S-M" or "M" offsets.
San-Andreas-(Carrizo)-rev	1857 A.D.	1	6	5.2	0.8	9.5	5.2	0.8	Cluster of offsets included in mean produce double COPD peak. Maximum COPD peak based on tighter cluster of "M" offsets.
San-Andreas-(Carrizo)-rev	1857 A.D.	2	4	4.8	0.8	5.0	5.0	1.0	Good maximum COPD peak. COPD uncertainty based on width of curve.

Fault name (section name)	Last rupture	Subsection	Number of single-event offset measurements	Mean single-event offset (m)	Standard deviation ± (m)	All offset COPD maximum (m)	Best estimate (m)	Uncertainty (m)	Comments
San-Andreas-(Carrizo)-rev	1857 A.D.	3	3	4.2	0.6	7.8	4.2	0.6	Maximum COPD based on tight cluster of offsets. Mean includes more diffuse lower cluster of offsets. Lower cluster likely represents slip in the last event.
San-Andreas-(Carrizo)-rev	1857 A.D.	4	3	4.8	0.9	12.0	4.8	0.9	COPD broad and multi-peaked for lower offsets. Maximum COPD uses 'M" offsets. Mean best represents slip in last event.
San-Andreas-(Carrizo)-rev	1857 A.D.	5	5	5.1	0.6	6.2	6.2	1.0	Good maximum COPD peak. COPD uncertainty based on width of curve.
San-Andreas-(Carrizo)-rev	1857 A.D.	6	6	5.4	0.7	5.3	5.4	0.7	
San-Andreas-(Big-Bend)	1857 A.D.	1	1	5.0	0.8	5.0	5.0	0.8	Used single 'S' measurement.
San-Andreas-(Big-Bend)	1857 A.D.	2	3	4.9	0.6	5.5	5.5	1.0	Strong maximum COPD peak.
San-Andreas-(Big-Bend)	1857 A.D.	3	4	4.2	0.8	4.5	4.2	0.8	Mean better captures low offset values. Maximum COPD not very strong.
San-Andreas-(Big-Bend)	1857 A.D.	4	2	4.6	0.8	4.0	4.6	0.8	Weak maximum COPD based on only one measurement.
San-Andreas-(Big-Bend)	1857 A.D.	5	1	5.1	0.4	5.1	5.1	0.4	Used single 'S' measurement.
San-Andreas-(Mojave-N)	1857 A.D.	1	1	5.4	1.0	15.6	5.4	1.0	Used single 'S' measurement. COPD based on multiple 'S-M' or 'M' offsets.

Fault name (section name)	Last rupture	Subsection	Number of single-event offset measurements	Mean single-event offset (m)	Standard deviation ± (m)	All offset COPD maximum (m)	Best estimate (m)	Uncertainty (m)	Comments
San-Andreas-(Mojave-N)	1857 A.D.	2	3	4.7	0.8	6.6	6.6	1.0	Strong maximum COPD peak.
San-Andreas-(Mojave-N)	1857 A.D.	3	1	5.6	0.5	5.6	5.6	0.5	Used single 'S' measurement.
San-Andreas-(Mojave-S)	1857 A.D.	2	8	4.6	0.7	5.7	5.7	1.0	Strong maximum COPD peak.
San-Andreas-(Mojave-S)	1857 A.D.	3	8	3.9	0.7	4.0	4.0	0.8	
San-Andreas-(Mojave-S)	1857 A.D.	4	2	3.3	0.6	2.9	3.3	0.6	Maximum COPD is part of a double peak. Mean better represents slip in last event.
San-Andreas-(Mojave-S)	1857 A.D.	7	2	2.9	0.7	3.0	3.0	0.7	
San-Andreas-(Mojave-S)	1857 A.D.	8	10	3.2	0.5	4.4	4.4	0.8	Good asymmetrical COPD peak
San-Andreas-(Mojave-S)	1857 A.D.	9	7	4.7	1.3	4.3	4.3	1.3	Good maximum COPD peak.
San-Andreas-(Mojave-S)	1857 A.D.	13	1	4.6	0.8	10.4	4.6	0.8	Used single 'S' measurement. COPD based on multiple "S-M" or "M" offsets.
San-Andreas-(Mojave-S)	1857 A.D.	14	1	4.3	0.7	4.3	4.3	0.7	Used single 'S' measurement.
San-Andreas-(Coachella)-rev	c. 1690 A.D.	3	4	3.3	1.1	5.9	3.3	1.1	

Fault name (section name)	Last rupture	Subsection	Number of single-event offset measurements	Mean single-event offset (m)	Standard deviation ± (m)	All offset COPD maximum (m)	Best estimate (m)	Uncertainty (m)	Comments
San-Andreas-(Coachella)-rev	c. 1690 A.D.	4	3	3.5	1.2	9.2	3.5	1.2	
San-Andreas-(Coachella)-rev	c. 1690 A.D.	5	6	3.0	0.8	2.6	2.6	0.8	Good maximum COPD peak.
San-Andreas-(Coachella)-rev	c. 1690 A.D.	6	3	2.2	0.5	7.2	2.2	0.5	
San-Andreas-(Coachella)-rev	c. 1690 A.D.	9	2	3.4	0.6	6.2	3.4	0.6	
San-Andreas-(Coachella)-rev	c. 1690 A.D.	10	6	3.0	0.8	3.9	3.9	1.0	
San-Cayetano	Post 1660 A.D.	0	1	4.3	1.0	4.9	4.3	1.0	Used single 'S' measurement.
San-Gregorio-(North)-2011-CFM	1270 A.D. - 1775 A.D.	8	2	4.0	2.9	3.0	5.0	+6/-2	Used slip in last event from a paleoseismic study (Simpson and others, 1997).
San-Jacinto-(Anza)-rev	1790 A.D.	1	48	1.9	0.6	1.2	1.2	0.6	
San-Jacinto-(Anza)-rev	1790 A.D.	2	37	2.5	0.6	1.6	1.6	1.0	
San-Jacinto-(Anza)-rev	1790 A.D.	3	8	3.6	0.6	3.4	3.6	1.0	
San-Jacinto-(Anza)-rev	1790 A.D.	4	59	2.7	0.4	3.4	2.7	0.4	

Fault name (section name)	Last rupture	Subsection	Number of single-event offset measurements	Mean single-event offset (m)	Standard deviation ± (m)	All offset COPD maximum (m)	Best estimate (m)	Uncertainty (m)	Comments
San-Jacinto-(Anza)-rev	1790 A.D.	5	56	2.8	0.5	3.1	2.8	0.5	
San-Jacinto-(Clark)-rev	1790 A.D.	0	48	2.8	0.5	2.7	2.8	0.5	
San-Jacinto-(Clark)-rev	1790 A.D.	1	121	2.5	0.4	2.6	2.5	0.4	
San-Jacinto-(Clark)-rev	1790 A.D.	4	22	1.3	0.3	1.4	1.3	0.3	
Simi-Santa-Rosa	Unknown	6	1	0.9	0.3	0.9	0.9	0.3	Used single 'S' measurement.

Table R6. "Best" estimate of displacement for the last event for UCERF 3 fault subsections: older historical and prehistoric ruptures.
["Older historical and prehistoric ruptures" are defined as all ruptures where offset measurements are based on geomorphology and paleoseismology; offsets for the creeping and Coachella sections of the San Andreas fault are maximum values because they include slip in the last event plus creep since the last event; calendar ages for events from UCERF3 appendix G; see appendix G for event-age references. BP, before present]

Fault name (section name)	Sub-section	Best estimate of offset (m)	Uncertainty + (m)	Uncertainty - (m)	Calendar age A.D. old (calibrated 2-sigma)	Calendar age A.D. young (calibrated 2-sigma)	Age BP max	Age BP min	Notes
Blackwater	8	2.0	0.1	0.1					No age data
Calico-Hidalgo	11	1.6	0.4	0.4			2000	600	
Calico-Hidalgo	12	1.9	0.4	0.4			2000	600	
Chino-alt-2	1	2.5	0.4	0.4			14200		
Compton	2	2.4	0.8	0.6			1750	700	
Elsinore-(Julian)	5	2.0	0.3	0.3			1700	700	
Elsinore-(Julian)	7	1.6	0.3	0.3			1700	700	
Elsinore-(Temecula)-rev	4	1.8	0.5	0.5	1655	1810			
Elsinore-(Temecula)-rev	5	2.0	0.5	0.5	1655	1810			
Garlock-(Central)	11	2.8	1.0	1.0	1450	1640			
Garlock-(Central)	14	2.9	0.6	0.6	1450	1640			
Garlock-(Central)	15	3.5	0.6	0.6	1450	1640			
Garlock-(Central)	16	2.5	1.3	1.3	1450	1640			
Garlock-(Central)	17	2.7	0.8	0.8	1450	1640			
Garlock-(Central)	18	2.8	0.8	0.8	1450	1640			
Garlock-(East)	4	3.6	0.5	0.5	1490				
Garlock-(East)	5	3.2	1.0	1.0	1490				
Garlock-(East)	6	2.5	0.9	0.9	1490				
Garlock-(East)	7	2.9	0.5	0.5	1490				
Garlock-(West)	2	3.5	1.5	1.5	1520	1850			
Garlock-(West)	6	2.7	1.9	1.9	1520	1850			
Garlock-(West)	7	2.8	0.8	0.8	1520	1850			
Garlock-(West)	10	3.9	1.0	1.0	1520	1850			
Garlock-(West)	11	1.9	0.8	0.8	1520	1850			
Garlock-(West)	12	2.0	0.8	0.8	1520	1850			
Garlock-(West)	13	2.6	0.7	0.7	1520	1850			

Fault name (section name)	Sub-section	Best estimate of offset (m)	Uncertainty + (m)	Uncertainty - (m)	Calendar age A.D. old (calibrated 2-sigma)	Calendar age A.D. young (calibrated 2-sigma)	Age BP max	Age BP min	Notes
Green-Valley-2011-CFM	5	1.4	0.2	0.2	1510	1721			
Hunter-Mountain-Saline-Valley	7	2.0	0.5	0.5					
Incline-Village-2011-CFM	2	2.8	0.5	0.5	1299	1444			
Lenwood-Lockhart-Old-Woman-Springs	7	2.4	0.5	0.5			2000	1600	
Lenwood-Lockhart-Old-Woman-Springs	8	3.5	0.5	0.5			2000	1600	
Lenwood-Lockhart-Old-Woman-Springs	9	3.7	0.5	0.5			2000	1600	
Little-Salmon-(Onshore)	1	4.4	0.8	0.8	1512	1800			
Little-Salmon-(Onshore)	2	5.6	0.5	0.5	1512	1800			
North-Frontal--(West)	5	1.7	0.5	0.5			11170		
Owens-Valley	4	2.2	0.9	0.9	1872	1872			
Owens-Valley	9	2.0	0.8	0.8	1872	1872			
Owens-Valley	14	2.3	1.1	1.1	1872	1872			
Owens-Valley	15	3.1	1.0	1.0	1872	1872			
Panamint-Valley	5	3.3	0.5	0.5	1400	1500			
Panamint-Valley	6	3.0	0.5	0.5	1400	1500			
Puente-Hills-(Santa-Fe-Springs)	1	3.0	0.7	0.7			300	200	
Rodgers Creek-Healdsburg-2011-CFM	2	2.0	0.3	0.3	1690				
Rodgers-Creek---	8	1.0	0.5	0.5	1690				

Fault name (section name)	Sub-section	Best estimate of offset (m)	Uncertainty + (m)	Uncertainty - (m)	Calendar age A.D. old (calibrated 2-sigma)	Calendar age A.D. young (calibrated 2-sigma)	Age BP max	Age BP min	Notes
Healdsburg-2011-CFM									
San-Andreas-(North-Coast)-2011-CFM	3	3.1	0.3	0.3	1906	1906			
San-Andreas-(North-Coast)-2011-CFM	15	3.6	0.5	0.5	1906	1906			
San-Andreas-(North-Coast)-2011-CFM	16	3.2	0.5	0.5	1906	1906			
San-Andreas-(Peninsula)-2011-CFM	6	3.7	0.7	0.7	1906	1906			
San-Andreas-(Creeping-Section)-2011-CFM	1	3.2	0.4	0.4	1906?	1906?			
San-Andreas-(Creeping-Section)-2011-CFM	3	3.9	0.3	0.3					
San-Andreas-(Creeping-Section)-2011-CFM	4	2.1	0.2	0.2					
San-Andreas-(Creeping-Section)-2011-CFM	18	2.9	0.4	0.4					
San-Andreas-(Cholame)-rev	6	3.7	0.7	0.7	1857	1857			
San-Andreas-(Cholame)-rev	7	4.5	1.0	1.0	1857	1857			
San-Andreas-(Cholame)-rev	8	3.4	0.7	0.7	1857	1857			
San-Andreas-(Cholame)-rev	9	3.9	0.9	0.9	1857	1857			
San-Andreas-(Cholame)-rev	10	1.4	0.3	0.3	1857	1857			

Fault name (section name)	Sub-section	Best estimate of offset (m)	Uncertainty + (m)	Uncertainty - (m)	Calendar age A.D. old (calibrated 2-sigma)	Calendar age A.D. young (calibrated 2-sigma)	Age BP max	Age BP min	Notes
San-Andreas-(Carrizo)-rev	0	5.0	0.8	0.8	1857	1857			
San-Andreas-(Carrizo)-rev	1	5.2	0.8	0.8	1857	1857			
San-Andreas-(Carrizo)-rev	2	5.0	1.0	1.0	1857	1857			
San-Andreas-(Carrizo)-rev	3	4.2	0.6	0.6	1857	1857			
San-Andreas-(Carrizo)-rev	4	4.8	0.9	0.9	1857	1857			
San-Andreas-(Carrizo)-rev	5	6.2	1.0	1.0	1857	1857			
San-Andreas-(Carrizo)-rev	6	5.4	0.7	0.7	1857	1857			
San-Andreas-(Big-Bend)	1	5.0	0.8	0.8	1857	1857			
San-Andreas-(Big-Bend)	2	5.5	1.0	1.0	1857	1857			
San-Andreas-(Big-Bend)	3	4.2	0.8	0.8	1857	1857			
San-Andreas-(Big-Bend)	4	4.6	0.8	0.8	1857	1857			
San-Andreas-(Big-Bend)	5	5.1	0.4	0.4	1857	1857			
San-Andreas-(Mojave-N)	1	5.4	1.0	1.0	1857	1857			
San-Andreas-(Mojave-N)	2	6.6	1.0	1.0	1857	1857			
San-Andreas-(Mojave-N)	3	5.6	0.5	0.5	1857	1857			
San-Andreas-(Mojave-S)	2	5.7	1.0	1.0	1857	1857			
San-Andreas-(Mojave-S)	3	4.0	0.8	0.8	1857	1857			
San-Andreas-	4	3.3	0.6	0.6	1857	1857			

Fault name (section name)	Sub-section	Best estimate of offset (m)	Uncertainty + (m)	Uncertainty - (m)	Calendar age A.D. old (calibrated 2-sigma)	Calendar age A.D. young (calibrated 2-sigma)	Age BP max	Age BP min	Notes
(Mojave-S)									
San-Andreas-(Mojave-S)	7	3.0	0.7	0.7	1857	1857			
San-Andreas-(Mojave-S)	8	4.4	0.8	0.8	1857	1857			
San-Andreas-(Mojave-S)	9	4.3	1.3	1.3	1857	1857			
San-Andreas-(Mojave-S)	13	4.6	0.8	0.8	1857	1857			
San-Andreas-(Mojave-S)	14	4.3	0.7	0.7	1857	1857			
San-Andreas-(Coachella)-rev	3	3.3	1.1	1.1	1657	1713			
San-Andreas-(Coachella)-rev	4	3.5	1.2	1.2	1657	1713			
San-Andreas-(Coachella)-rev	5	2.6	0.8	0.8	1657	1713			
San-Andreas-(Coachella)-rev	6	2.2	0.5	0.5	1657	1713			
San-Andreas-(Coachella)-rev	9	3.4	0.6	0.6	1657	1713			
San-Andreas-(Coachella)-rev	10	3.9	1.0	1.0	1657	1713			
San-Cayetano	0	4.3	1.0	1.0	1660				
San-Gregorio-(North)-2011-CFM	8	5.0	6.0	2.0	1270	1775			
San-Jacinto-(Anza)-rev	1	1.2	0.6	0.6	1740	1800			
San-Jacinto-(Anza)-rev	2	1.6	1.0	1.0	1740	1800			
San-Jacinto-(Anza)-rev	3	3.6	1.0	1.0	1740	1800			
San-Jacinto-(Anza)-rev	4	2.7	0.4	0.4	1740	1800			
San-Jacinto-(Anza)-rev	5	2.8	0.5	0.5	1740	1800			

Fault name (section name)	Sub-section	Best estimate of offset (m)	Uncertainty + (m)	Uncertainty - (m)	Calendar age A.D. old (calibrated 2-sigma)	Calendar age A.D. young (calibrated 2-sigma)	Age BP max	Age BP min	Notes
San-Jacinto-(Clark)-rev	0	2.8	0.5	0.5	1790	1790			Best estimate
San-Jacinto-(Clark)-rev	1	2.5	0.4	0.4	1790	1790			Best estimate
San-Jacinto-(Clark)-rev	4	1.3	0.3	0.3	1790	1790			Best estimate
Simi-Santa-Rosa	6	0.9	0.3	0.3					No age data

Table R7. Repeated slip for a subsection from cumulative offset probability distributions for offset features.

[1-6, event order with 1 indicating most recent event and 6 representing the sixth-oldest event; MRE, most recent event; PEN, penultimate event; + and -, uncertainties representing half-width of COPD peak; for asymmetrical uncertainties, we conservatively use larger uncertainty in weighted mean calculation; yellow, preferred offsets using only the tallest and sharpest cumulative offset probability density (COPD) peaks; white, alternate offsets that incorporate smaller and broader COPD peaks, including shoulders on larger peaks; gray, no data; italics denote weak COPD peaks that may not represent entire slip from one event; figures showing COPD curves used to estimate repeated slip for each subsection in supplemental files R7]

Fault	Section	Sub-section	Event slip and uncertainty (m)																				
			1 (MRE)	+	-	2 (PEN)	+	-	3	+	-	4	+	-	5	+	-	6	+	-	Weighted mean	+	-
San Andreas rev	Carrizo	1	**4.5**	0.2	0.5	**1.3**	0.7	0.4	**3.8**	0.7	0.7										3.5	0.4	0.4
			5.1	1	0.8	**4.4**	0.7	0.7													4.6	0.6	0.6
San Andreas rev	Carrizo	5	**6.2**	0.8	0.5	**3.1**	0.5	0.8	**2.2**	1	0.5										4.1	0.5	0.5
San Andreas rev	Carrizo	6	**5.4**	0.8	0.5	**4.9**	0.6	1.8	**2.7**	1.2	0.7										4.6	0.6	0.6
San Andreas	Cholame	8	**3.9**	0.4	0.7	**1.5**	0.6	0.4													2.5	0.5	0.5
			2	0.2	0.2	**1.8**	0.4	0.7	**1.5**	0.6	0.4										1.9	0.2	0.2
San Andreas rev	Coachella	4	**3.5**	0.3	0.9	**3**	0.6	0.6	**2.7**	0.7	0.7	***2.5***	3.2	0.6							3.0	0.4	0.4
San Andreas rev	Coachella	10	**3.8**	0.7	0.6	**3**	0.5	0.9	**2**	0.8	0.5	**3.4**	0.9	0.8	**3.7**	0.9	0.9				3.2	0.4	0.4
San Andreas	Mojave S	2	**3.5**	0.4	0.5	**2.2**	0.9	0.7	***2.6***	0.4	0.4										2.9	0.3	0.3
San Andreas	Mojave S	3	**4**	0.3	0.9	**2.3**	0.3	0.4	**4.9**	1	1										2.9	0.3	0.3
Elsinore	Julian	5	**1.2**	0.1	0.1	**0.8**	0.2	0.1													1.1	0.1	0.1
			0.82	0.1	0.1	**0.4**	0.1	0.1	**0.8**	0.2	0.1										0.6	0.1	0.1
Garlock	West	10	**4**	1	0.7	**5.5**	1.1	0.7													4.7	0.7	0.7
			2.3	0.4	1.4	**1.7**	1	0.7	**3.4**	0.8	1.3	**2**	1.1	0.7							2.2	0.6	0.6
Garlock	West	12	**2.4**	0.9	0.9	**3.2**	0.7	0.7	**2.9**	1	0.8	**4.8**	1	1.2	**4**	0.6	0.4				3.5	0.4	0.4

Fault	Section	Sub-section	Event slip and uncertainty (m)																			
			1 (MRE)	+	-	2 (PEN)	+	-	3	+	-	4	+	-	5	+	-	6	+	-	Weighted mean	+	-
Garlock	Central	15	**3.5**	0.4	0.5	**2.5**	0.5	0.8	**2.5**	1	0.5										3.1	0.4	0.4
San Jacinto rev	Anza	1	**1.2**	0.6	0.5	**2.6**	0.5	0.7	**2**	0.4	0.5	**1.8**	0.7	0.5							1.9	0.3	0.3
San Jacinto rev	Anza	5	***1.2***	0.2	0.3	**1.9**	0.6	0.8	**2.7**	0.7	0.8										1.4	0.3	0.3
			3.1	0.6	0.8	**2.7**	0.7	0.8													2.9	0.6	0.6
San Jacinto rev	Clark	0	**2.7**	1	0.9	**3.4**	1.4	0.8													2.9	0.8	0.8
			1.6	0.3	0.6	**1.1**	1	0.9	**1.9**	0.7	0.4	**1.5**	1.4	0.8							1.6	0.4	0.4
San Jacinto rev	Clark	1	**2.6**	0.1	0.1	**2.8**	0.03	0.1	**2.1**	0.1	0.04										2.5	0.1	0.1
San Jacinto rev	Clark	4	**1.4**	0.3	0.3	**1.4**	0.2	0.3	**1.1**	0.3	0.3										1.3	0.2	0.2

Table R8. Repeated slip at a point from paleoseismology.

[1-6, event order with 1 indicating most recent event and 6 representing the sixth-oldest event; MRE, most recent event; PEN, penultimate event; + and -, measurement or model uncertainties]

Fault	Latitude	Longitude	1 (MRE)	+	-	2 (PEN)	+	-	3	+	-	4	+	-	5	+	-	6	+	-	Mean	+	-
Compton[1]	33.965991	-118.262921	2.4	0.8	0.6	3.7	1.5	1.2	2.5	1.1	0.9	2.7	0.9	0.8	1.3	0.6	0.5	4.2	1	0.8	2.8	0.5	0.3
Puente Hills[2]	33.905282	-118.110351	2.4	0.5	0.5	2.4	0.4	0.4	3.5	0.9	0.9										2.8	0.4	0.4
Puente Hills[2]	33.905069	-118.111422	3.5	0.9	0.9	2.4	0.3	0.3	2.9	0.6	0.6										2.9	0.4	0.4
San Andreas rev[3]	35.269206	-119.825108	7.9	0.1	0.1	7.6	0.4	0.4	5.2	0.6	0.6	1.4	0.5	0.5	8	0.5	0.5				5.4	0.2	0.2
San Andreas rev[4]	34.370541	-117.668229	1.0-2.0			3.0-5.0			3.0-5.0												2.3-4.0		
San Andreas rev[5]	34.45584	-117.887651	5.5	3	3	6.25	1	1	6.25	1	1										6.0	0.7	0.7

[1]Leon and others, 2009.

[2]Leon and others, 2007.

[3]Liu and others, 2004; Liu-Zeng and others, 2006.

[4]Weldon and others, 2002; slip for events 2 and 3 derived by dividing 6-10 m of slip over two events by two.

[5]Salyards and others, 1992; 1-m uncertainties applied to events 2 and 3.

Table R9. Average displacement for selected large ruptures from geomorphology.

Fault	Date	Length (km)	Ave disp. (m)	Data type and source	Other estimates
Garlock	1450-1640	248	1.7–4.3	LiDAR (this investigation); Field (McGill and Sieh, 1991)	
Owens Valley	1872	90–110	1.0–2.9	LiDAR (this investigation)	Appendix F, this report: 110 km, 2.5 m
San Jacinto	1550	85–120	2.7	LiDAR, field, aerial photo (Salisbury and others, 2012)	Appendix F, this report: 110 km, 2.5 m
San Jacinto	1880	85–120	~2.7	LiDAR, field, aerial photo (Salisbury and others, 2012)	Appendix F, this report: 80 km, 2.0 m
San Andreas	Circa 1700s				Appendix F, this report: 230km, 3.5 m
San Andreas	Circa 1690	220–240	2.3–3.0		Appendix F, this report: 235 km, 4 m
San Andreas	12/1812				Appendix F, this report: 230km, 2.3 m
San Andreas	1/9/1857	320–360+	4.3	LiDAR (Zielke and others, 2012); Field (Sieh, 1978); Field, aerial photo (Lienkaemper, 2001); Paleoseismology (various)	Appendix F, this report: 339 km, 4.45 m; Zielke and others (2012) : 350 km, <3.5 m; Sieh (1978): 360-400+, 4.5-4.8 m; Wesnousky (2008): 360 km, 4.7 m.

Supplementary Files

R1. Offset Database
- R1-1. Offset Compilation Table
- R1-2. Fault Location and Offset Figures
- R1-3. KML Files

R2. New Offset Measurements—Methodology and Description
- R2-1. Measuring Earthquake-Generated Surface Offsets from High-Resolution Topography
- R2-2. Description of New Offset Measurements Generated for UCERF3 Slip in Last Event Database

R3. Measurement and Feature Quality

R4. Analysis Tools—Matlab Codes and Scripts

R5. Input Tables for Analysis Tools
- R5-1 Fault Segments

R5-2 Geodetic
R5-3 Offset Data

R6. Analysis Output

R6-1 Faults with Slip
R6-2 Offsets by Fault and Subsection and Type
R6-3 Results - Calculated Mean and Standard Deviation and COPD for Subsections
R6-4 Figures

R7. COPD Offsets